INFORMATION TO USERS

This manuscript has been reproduced from the microfilm master. UMI films the text directly from the original or copy submitted. Thus, some thesis and dissertation copies are in typewriter face, while others may be from any type of computer printer.

The quality of this reproduction is dependent upon the quality of the copy submitted. Broken or indistinct print, colored or poor quality illustrations and photographs, print bleedthrough, substandard margins, and improper alignment can adversely affect reproduction.

In the unlikely event that the author did not send UMI a complete manuscript and there are missing pages, these will be noted. Also, if unauthorized copyright material had to be removed, a note will indicate the deletion.

Oversize materials (e.g., maps, drawings, charts) are reproduced by sectioning the original, beginning at the upper left-hand corner and continuing from left to right in equal sections with small overlaps. Each original is also photographed in one exposure and is included in reduced form at the back of the book.

Photographs included in the original manuscript have been reproduced xerographically in this copy. Higher quality 6" x 9" black and white photographic prints are available for any photographs or illustrations appearing in this copy for an additional charge. Contact UMI directly to order.

UMI

A Bell & Howell Information Company
300 North Zeeb Road, Ann Arbor MI 48106-1346 USA
313/761-4700 800/521-0600

Université d'Ottawa · University of Ottawa

STRUCTURAL STUDIES OF ANTI-TUMOUR ANTIBODY R24

Marcin Jerzy Kaminski

Thesis submitted to the
Department of Biochemistry, Microbiology and Immunology
in partial fulfilment of the requirements for the degree of
Master of Science

University of Ottawa

Ottawa, Ontario, Canada

May, 1998

ABSTRACT: The murine monoclonal antibody R24 and mouse-human Fv-IgG1(κ) chimeric monoclonal antibody chR24 are specific for the cell surface tumour antigen disialoganglioside GD3. X-ray diffraction and surface plasmon resonance experiments have been employed to study the mechanism of "homophilic binding" in which molecules of R24 recognize and bind to other molecules of R24 through the heavy chain variable domains. The relationship between GD3-binding and the homophilic-binding domain, and the mechanism of the behaviour of chR24 mutants has also been investigated. R24 exhibits strong binding to GD3-bearing liposomes, with no apparent binding saturation, while chR24 binding is much weaker. This suggests that cooperative interactions involving antibody constant regions contribute to R24 binding to membrane-anchored GD3. The crystal structures of the Fabs from R24 and chR24 reveal the mechanism for homophilic binding and confirm that the homophilic and antigen-binding idiotopes are distinct. The homophilic binding idiotope is formed largely by an antiparallel β-sheet dimerization between the H2 CDR loops of two Fabs, while the antigen-binding idiotope is a pocket formed by the three CDR loops of the heavy chain. The conformation of the antigen-binding site explains why mutations of specific residues blocks GD3-binding. Comparison with known structures of other Fabs shows that the formation of homophilic dimers requires the presence of a canonical conformation for the H2 CDR in conjunction with side chain participation. The relative positions of the homophilic and antigen binding sites allows for a lattice of R24 antibodies to be constructed, which is stabilized by the presence of the cell membrane. The model provides for the selective recognition cells which overexpress GD3 on the membrane surface by R24.

DEDICATION

To my parents who instilled in me a curiosity for the world, and supported my interest in the sciences. Their contributions to my education will never be forgotten.

ACKNOWLEDGEMENTS

I would like to thank all the individuals that have helped me during this project. First and foremost I would like to thank Dr. Stephen Evans for his guidance, patience, humour and all of the knowledge and ideas that I was able to gain during my experience in X-ray crystallography. I thank Dr. C. Roger MacKenzie and Tomoko Hirama for carrying out the surface plasmon resonance experiments. I would also like to thank Sonia Patenaude who not only helped me in the lab, but was always there to make sure I was working to full capacity, and Dr. Marilyn Mooibroek, who's knowledge and level-headedness proved invaluable during laboratory experiments. I would like to thank Rebecca To, for showing me the basics of crystal mounting. I also thank Dr. Z. C. Jia at Queens University, Kingston, Ontario, Canada, for access to his data collection equipment and assistance with the data collection. Joanne Barlow and Julie Normand were a great support in all my dealings with the University management.

DECLARATION

I certify that this thesis does not include, without acknowledgement any material previously submitted for a degree at any university. To the best of my knowledge and belief, this thesis does not contain any material previously published or written by another except where due reference is made in text.

I authorize the University of Ottawa to reproduce this thesis in total or in part at the request of another institution for academic research.

Marcin Jerzy Kaminski

TABLE OF CONTENTS

APPENDIX A: Abbreviations

A_{280}	Absorbance at wavelength of 280 nm
Ab	Antibody
Ag	Antigen
B	Temperature factor
BEC2	Murine monoclonal antibody BEC2
BIA	Biospecific interaction analysis
C	C-terminus of IgG
CDR	Complementarity Determining Region
C_{H1}	Antibody heavy chain constant domain 1
C_{H2}	Antibody heavy chain constant domain 2
C_{H3}	Antibody heavy chain constant domain 3
chR24	Human-mouse chimeric monoclonal antibody R24
C_L	Antibody light chain constant domain
CS I	Hampton Incomplete Factorial Crystal Screen I solutions.
CS II	Hampton Incomplete Factorial Crystal Screen II solutions.
Da	Dalton(s)
ELISA	Enzyme-Linked Immunosorbent Assay
F	Structure factor
Fab	Fragment with antigen binding
Fab'	Symmetry related Fab molecule of chR24 crystal structure

Fab1'	Symmetry related Fab1 molecule of R24 crystal structure
Fab2'	Symmetry related Fab2 molecule of R24 crystal structure
Fc	Fragment which crystallized
Fc	Calculated structure factor
Fo	Observed structure factor
FPLC	Fast protein liquid chromatography
Fv	Variable region of the Fab (or IgG) comprised of V_L and V_H
Gal	Galactose
GD3	Disialogangloside consisting of : Glc-Gal-Neu5Ac-Neu5Ac
Glc	Glucose
HgPapain	Mercuripapain suspension (inactive enzyme)
HPLC	High performance liquid chromatography
ID	Idiotope
ID_{GD3}	GD3 binding idiotope
ID_{HOM}	Homophilic binding idiotope
IEF-PAGE	Iso electric focusing polyacrylamide gel electrophoresis
IgA	Immunoglobulin A
IgD	Immunoglobulin D
IgG	Immunoglobulin G
IgM	Immunoglobulin M
mAb	Monoclonal antibody
N	N-terminus of IgG

Neu5Ac	N-acetyl Neuraminic Acid (*also* Sialic Acid)
NeuGl	N-glycolyl Neuraminic Acid
PDB	Protein Data Bank
PEG	Polyethylene glycol
R24	Murine monoclonal antibody R24
SDS-PAGE	Sodiumdodecyl sulfate polyacrylamide gel electrophoresis
SPR	Surface plasmon resonance
$\bar{u}$	Mean thermal displacement (Å)
V_H	Antibody heavy chain variable domain
V_L	Antibody light chain variable domain

1 INTRODUCTION:

1.1 Overview

1.1.1 Problem

Immunotherapy utilizes methodologies which exploit the immune system to neutralize diseased cells and disease-causing organisms. Immunotherapy employed against cancers includes treatment with monoclonal antibodies (mAb) which recognize tumour antigens (Ag). Research has concentrated on human melanoma malignancies and both humoral and cellular immune responses specific to melanoma antigens have been reported (Dippold *et al.*, 1980; Lloyd, 1993; Boon, 1993; Cole *et al.*, 1995). To date few antigens have been identified which are recognized by both components of the immune system, which reduces the efficacy of the therapeutical applications since the immune response is optimized when both components can be brought to bear on the cancer. Research on humoral mediated recognition of melanoma antigens has identified at least six antigens, four of which have been found to be gangliosides (Lloyd, 1993). Gangliosides consist of two basic units: a hydrophobic ceramide moiety and a hydrophilic oligosaccharide (Hakomori, 1981). The lipid moiety is sequestered within the membrane and is not targeted by the immune system, leaving the hydrophilic carbohydrate moiety exposed to immune surveillance. The presence of gangliosides on noncancerous tissues does present some difficulties in immunotherapy, however these factors are overcome by the density of glycosphingolipids expressed on malignant cells and by the diversity of available antigens (Irie and Rawindranath, 1990). One method currently of interest both clinically and in basic research is the exploitation of specific cell-surface tumour markers

in order to develop specific monoclonal antibodies as therapeutic agents (Albino *et al.*, 1986). Certain mAb isotypes are used to induce complement activation at cells in the tumour, leading to tumour cell death. The development of mAbs specific to gangliosides has presented a few problems, as they are carbohydrate antigens and as such are not T-cell dependent. Further, like many carbohydrates, they are often poorly immunogenic.

The relative abundance of certain gangliosides on the cell surface can change during cancerous mutation, and the over-expression of each type of ganglioside on a cell provides a new venue for antibody mediated cancer therapy (Carubia *et al.*, 1984; Albino, *et al.* 1986). An example of such a ganglioside is GD3 (Figure 1), which is over

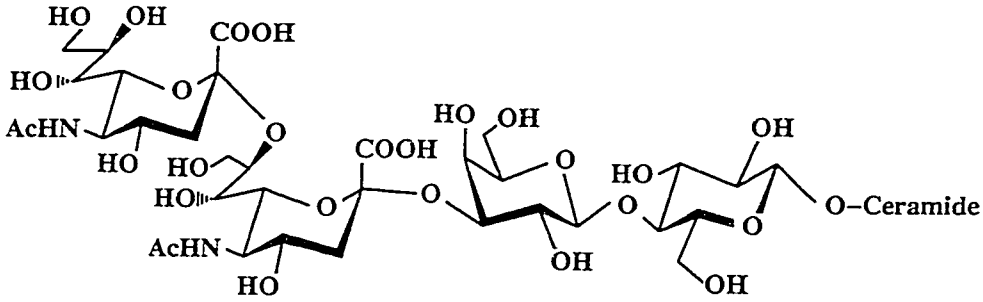

GD3 – NeuAc : Neu5Ac α2–8 Neu5Ac α2–3 Gal β1–4 Glu–Ceramide

Figure 1: Schematic of GD3 ganglioside structure. The four residue poly-saccharide chain is linked to a ceramide lipid moiety which anchors the glycosphingolipid in the cell membrane.

expressed on melanomas, soft tissue sarcomas and tumours of neuroectodermal origin, while normal tissues display little or no GD3 (Hamilton *et al.*, 1993). Various "substituted" GD3 types have been identified (Table 1.1), and all contain a modification of one of the N-acetyl neuraminic acid residues (Pukel *et al.*, 1982; Thurin *et al.*, 1985; Hirabayashi *et al.*, 1987).

TABLE 1.1: Ganglioside GD3 forms and distribution (Irie and Rawindranath, 1990).

GD3 type	Terminal residue structure	Normal distribution	Malignant distribution
GD3 - NeuAc	Neu5Ac-α(2→8)-Neu5Ac*	milk, retina, dura matter, thymus, dermis, thyroid, aorta intima, serum, kidney	melanoma, glioblastoma, astrocytoma, meningloma, neurofibrosarcoma, leukemia, thyroid cancer
GD3 - NeuGl	NeuGl-α(2→8)-Neu5Ac* Neu5Ac-α(2→8)-NeuGl*	no report	melanoma
GD3 - O-Ac-NeuAc	O-Ac-Neu5Ac-α(2→8)-Neu5Ac*	no report	melanoma

* These terminal residues are linked to Gal-β(1→4)-Glc-β(1→1)-Ceramide *via* an α(2→3) bond.

The best characterized GD3 type, GD3 - NeuAc consists of a ceramide lipid group with an Neu5Ac-Neu5Ac-Gal-Glc chain (Figure 2).

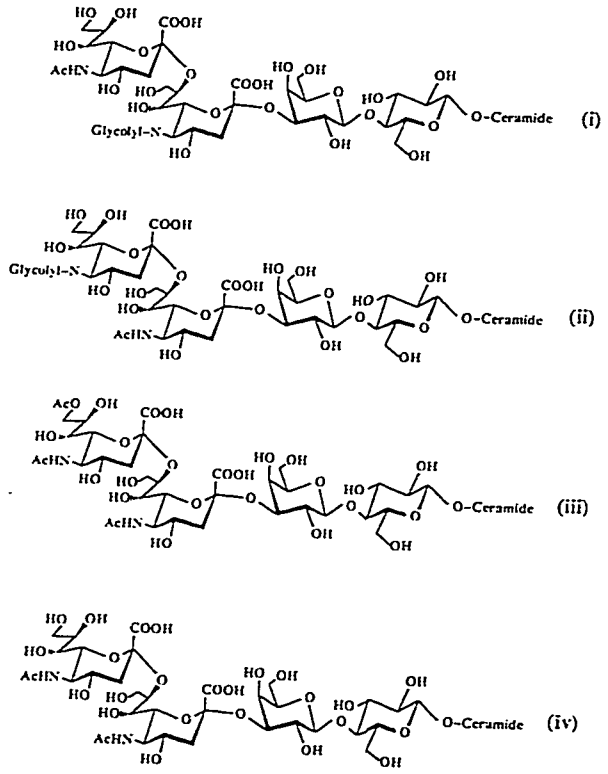

Figure 2: Schematic of carbohydrate arrangement of the four known GD3 ganglioside chains. Shown are the two terminal sialic acid residues linked to galactose and glucose: i); ii) GD3-NeuGl iii) GD3-O-Ac-NeuAc iv) GD3-NeuAc.

Several antibodies specific for GD3-NeuAc antigen have been identified, including mAb R24. R24 is a murine monoclonal antibody (Pukel *et al.*, 1982) and one of the most actively investigated anti-carbohydrate monoclonal antibodies in cancer therapy (A. N. Houghton, *personal communication*).

R24 has been shown to prevent tumour development in animal models (Chapman, *et al.* 1990), and to have anti-tumour activity in human clinical trials (Vadhan-Raj *et al.*, 1988; Caulfield *et al.*, 1990; Raymond *et al.*, 1991). R24 is unusual due to the display of "homophilic binding" (i.e. R24 binding R24) through the antigen binding site (Chapman *et al.*, 1990b), a feature possibly used for amplification of the immune response upon antigen-antibody binding.

Site-directed mutagenesis of R24 has been accomplished (Yan *et al.*, 1996) with mutations at the putative GD3 binding site causing a loss of homophilic binding as well. A striking feature of the binding site of the native and mutant R24 antibodies is the fact that homophilic binding is disrupted by mutations which do not prevent antigen specific interactions (Yan *et al.*, 1996). At present two forms of R24 are available for study; the native murine mAb, and the human-mouse chimeric mAb (chR24), described below.

In order to overcome the observed low immunogenicity of GD3, the formation of anti-idiotypic antibodies which carry an "internal image" of the antigen (see below for an explanation of an "internal image") has been attempted. Such anti-idiotypic antibodies, when used as vaccines can stimulate both the cellular and humoral portions of the immune system, and thus should induce a much stronger immune response than the carbohydrate antigen. One such anti-idiotypic antibody is BEC2, which has been shown

to induce formation of anti-GD3 antibodies in animal models and in preliminary clinical trials. This project deals with the determination of the structures of both R24 and chR24 antigen-binding site and homophilic-binding site, and how the antigen-binding site may be involved in GD3, BEC2 and homophilic interactions. Surface plasmon resonance experiments were carried out in collaboration with Dr. C. Roger MacKenzie at the Institute for Biological Sciences of the National Research Council. A comparison of the R24 and chR24 is carried out in order to determine if the humanization process, which increases the effectiveness of R24 as a therapeutic agent in humans, has had any effect on the avidity and affinity of the chimer. Finally, a model of the BEC2 Fv structure was constructed in order to explain how a protein (BEC2) can mimic a polysaccharide antigen (GD3) in its interaction with R24.

1.1.2 Antibody structure

Antibodies derive from the humoral component of the immune system. The complementary shape and attractive forces between the antibody and antigen are key to understanding the specificity of antibodies. The basic shape or structure on the antigen to which an antibody can bind is called the "epitope". The corresponding structure on the antibody molecule is called the "paratope". Most antigens will have more than one expressed epitope, and will thus cause the production of a series of antibodies, each specific to a single epitope. The interaction between Ab and Ag is epitope-specific, however, it is possible for an Ab to bind a related antigen, for example some anti-guinea fowl lysozyme antibodies can bind chicken lysozyme due to an interaction with a similar antigen epitope (Lescar *et al.*, 1995). This type of interaction is termed "cross-reactivity".

Antibodies or immunoglobulins are glycoproteins, composed of approximately 82-96% polypeptide chain, and 4-18% carbohydrate (Seymour, 1995). The immunoglobulins present *in vivo*, even those specific to one antigen, come from a series of source B cells and are termed polyclonal. In order to simplify studies and modifications of antibodies it is necessary to obtain a single clone source which would be capable of producing large amounts of the antibody. One method of accomplishing this is to fuse a myeloma cell (a cancerous plasma cell) with a lymphocyte. This process yields a hybridoma cell line which produces only one type of antibody, termed monoclonal antibody.

Human and mouse immunoglobulins are classified into five isotypes based on the heavy chains. The different heavy chain forms are labelled α, δ, ϵ, γ, μ giving the immunoglobulin classes IgA, IgD, IgE, IgG, and IgM respectively. The light chains come in two varieties classified as kappa (κ) and lambda (λ). The general shape of IgG's is a Y

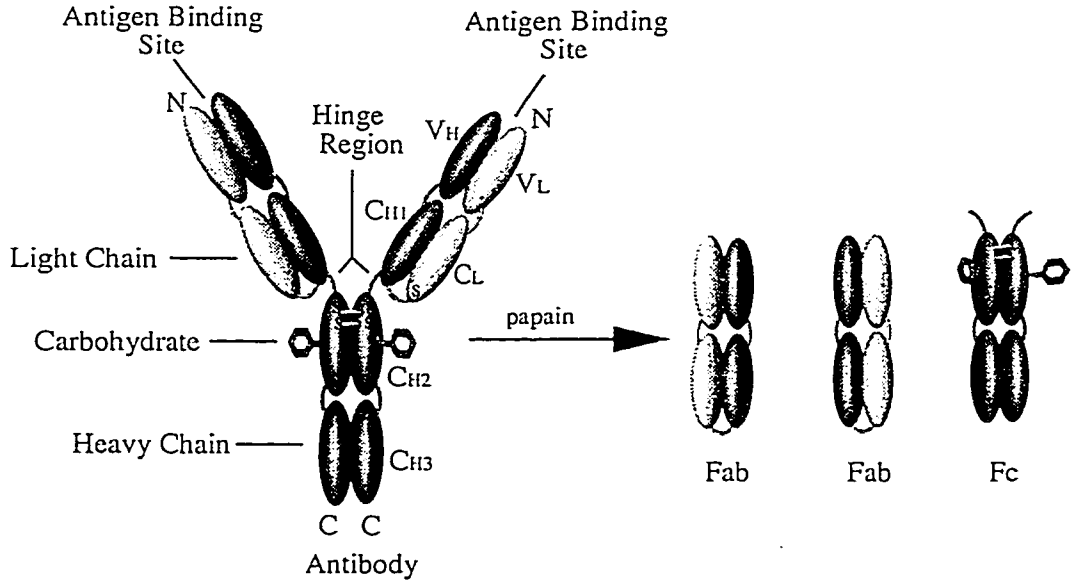

Figure 3: IgG structure. The IgG is made up of two light (white) and two heavy (black) chains, and can be separated through proteolytic cleavage into the Fc and Fab fragments. The Fab fragments contain the antigen binding sites and maintain activity at these sites. (Branden and Tooze, 1991)

structure consisting of two light (25,000 Da) and two heavy (50,000-65,000 Da) polypeptide chains (Figure 3). These chains generally have both inter- and intra-chain disulfide bridges. The molecule can be cleaved by papain into 3 fragments by cutting at the hinge regions which connect the arms of the Y to the tail (Porter, 1950). The two equivalent arm fragments are called Fabs and the tail portion, to which carbohydrate moieties are conjugated, is called the Fc.

The general structures of human and mouse antibodies are well understood. The N-terminal regions of each chain in the antibody have a higher degree of variability in the amino acid sequence than the regions proximal to the C terminus. These are respectively labelled the variable and constant regions (Poljak, 1973; Davies, 1988). The light chains consist of one variable (V_L) and one constant (C_L) domain, while heavy chains consist of one variable (V_H) and three constant (C_{H1}, C_{H2}, C_{H3}) domains. Each domain, whether constant or variable, is composed of a framework region: a tightly packed β-barrel built of two antiparallel β-sheets. Constant domain barrels have one four- and one three-stranded β-sheet. The length and sequence of constant domain loops is invariant in members of the same immunoglobulin class, but can vary greatly between classes. Variable domain β-barrels have one four- and one five-stranded β-sheet joined by loops. Three of these loops on each chain have highly-variable sequence and length and comprise the antigen-binding regions (Wu and Kabat, 1970). The hypervariable loops are

also called "*C*omplementarity *D*etermining *R*egions" (CDRs). V_L CDRs are labelled L1, L2 and L3 while V_H CDRs are labelled H1, H2, H3. These loops occur in both the heavy and light chains at approximately at residues 25-35 for L1 and H1, residues 50-65 for L2 and H2, and residues 90-105 for residues in L3 and H3 (Chothia *et al.*, 1989; Padlan, 1994). The amino acid sequence within these loops as well as the number of amino acids per loop determine the specificity of the given antibody (Figure 4).

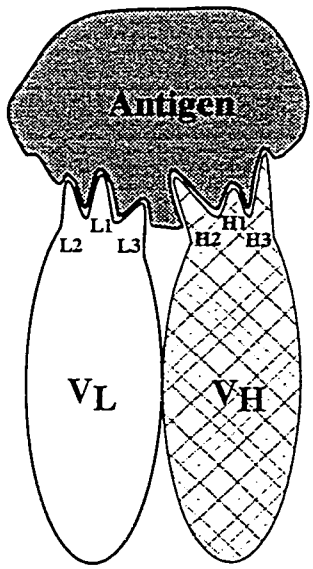

Figure 4: Fab antigen binding site. The hypervariable loops of the light and heavy chains form an epitope-specific structure which interacts with the antigen.

Modifications of the hypervariable loops will alter the outer appearance of the paratope, thereby altering the antibody-antigen interactions. In general both the V_L and V_H CDRs can be involved in binding of the antigen epitope. The constant regions are not usually active in the Ag-Ab interaction, but do participate in the activation of the complement pathway, interact with receptors on macrophages during phagocytosis, and participate in antibody-dependent cell-mediated cytotoxicity (Seymour et al., 1995).

IgG is the most prominent isotype of the immunoglobulin (Ig) families, forming about seventy-five percent of the total serum Ig concentration. Murine systems show four IgG subclasses IgG1, IgG2a, IgG2b, and IgG3. R24 is a member of the murine IgG3 family. Four human subclasses of IgG have been identified to date IgG1, IgG2, IgG3 and IgG4 (Tizard, 1984). IgGs are the major immunoglobulin produced in response to a previously encountered antigen. In humans, IgG1, IgG3, and IgG4 can also function as a source of temporary immunity for newborns by passing through the placental barrier. The four groups differ in the activity of the constant domains. IgG1, IgG2 and IgG3 can activate the classical complement pathway. IgG1 and IgG3 can also bind to macrophages in order to facilitate phagocytosis, while IgG2 and IgG4 interact with killer cells during antibody dependent cell-mediated cytotoxicity of Ab-bound cells.

The remaining antibody classes perform different functions. IgM is the major Ig of the primary immune response, and is also found in large proportions in lower animals. IgM occurs in a pentameric form *in vivo*, and participates in fixing complement in the classical pathway. IgM is also the main antigen-specific protein on B cell surfaces. IgA is found primarily in external secretions, and exists as a homodimer. IgA is actively transported through cells to the epithelium, where it is critical in prevention of penetration of this surface by pathogens. IgD is found on surfaces of B cells, and seems to occur in high amounts on naive B cells, that is cells which have not yet been recruited to fight a specific antigen. These cells undergo class switching when stimulated by an antigen, and produce IgG, IgA, and IgE immunoglobulins.

It is also possible to create antibodies through protein engineering. Such proteins

include chimers which are composed of parts of immunoglobulins from different species. This is the case with the mouse-human chimeric IgG chR24 which expresses the anti-GD3 idiotope. chR24 was constructed by ligating the mouse genes encoding V_H and V_L onto the human IgG1 C_H and C_L genes (Figure 5). This R24 variant was designed to

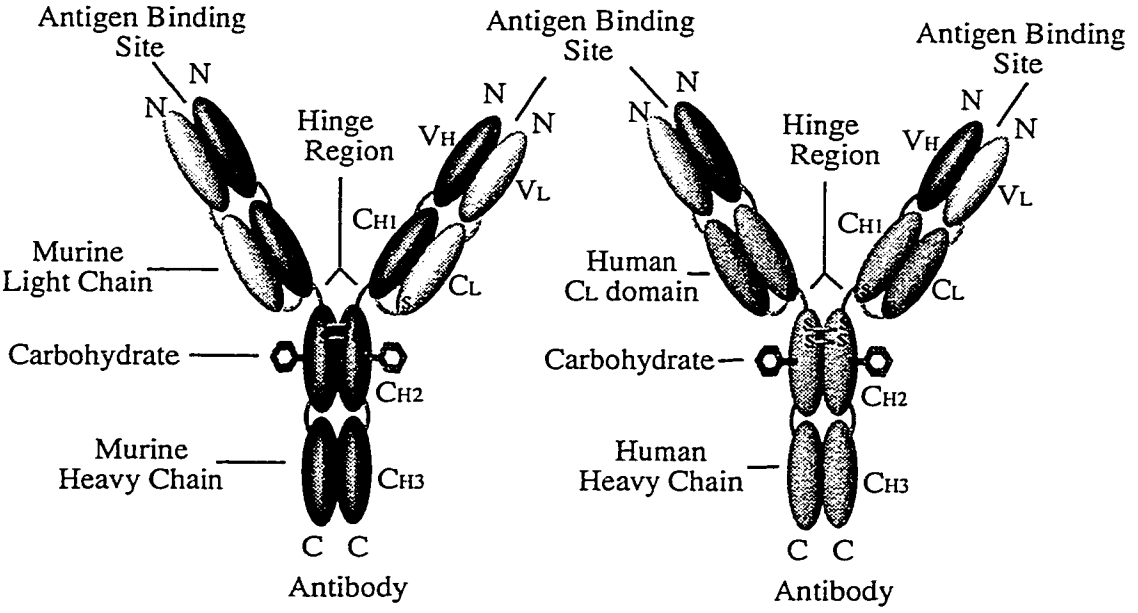

Figure 5: Comparison of murine and murine-human chimeric monoclonal antibodies. The murine protein is shown in white (light chain) and black (heavy chain); the human in gray. Each antibody has two antigen-binding regions at the N-terminal domains of the chains. The Fv portions of both antibodies are identical.

minimize human immune response against the murine R24 while maintaining its GD3-binding ability, thus improving therapeutic effectiveness of the IgG.

1.1.3 Antibody-Antigen Interactions

The complementarity of surfaces between the Ag epitope and the Ab paratope allows for close contact between relatively large surfaces of the two molecules. These contacts are not covalent in nature, but are based on four forces: electrostatic, van der

Waal's, hydrogen bonding, and hydrophobic interactions. Electrostatic interactions deal with the interactions of oppositely charged groups such as the carboxyl and amino groups which both the antigen and the antibody may contain. The attractive force between the opposite charges varies inversely with the square of the separation. Van der Waal's forces are much weaker than ionic interactions, and depend on dipole-dipole interactions which vary with the inverse of separation to the power of seven. This means that the force is negligible unless the atoms are in contact. Hydrogen bonding and hydrophobic interactions are complementary. Hydrogen bonding is a special form of dipole-dipole interactions, which occurs when a hydrogen bound to a highly electronegative atom (such as O and N) in a molecule interacts with another atom in the same or different molecule: N-H ••• O for example. Hydrogen interactions are in the 2-7 kcal/mol range, more than van der Waals interactions and much lower than chemical bond energies. Hydrophobic interactions occur when two relatively hydrophobic faces come together expelling water from the interface.

1.1.4 Idiotopes, Idiotypes, Antiidiotypes and Idiotypic Networks

In addition to their paratopes, antibody variable regions have been shown to express epitopes which act as targets for other members of the immunoglobulin supergene family (Patel, 1989; Lenert *et al.*, 1990). Some antibodies have also expressed

self or homophilic binding through these epitopes. Antibodies can induce the formation of "anti-antibodies", which in turn induce "anti-anti-antibodies" in an idiotypic network (Fig 6) (Jerne, 1974). The evolution of the idiotypic network theory has lead to the use of

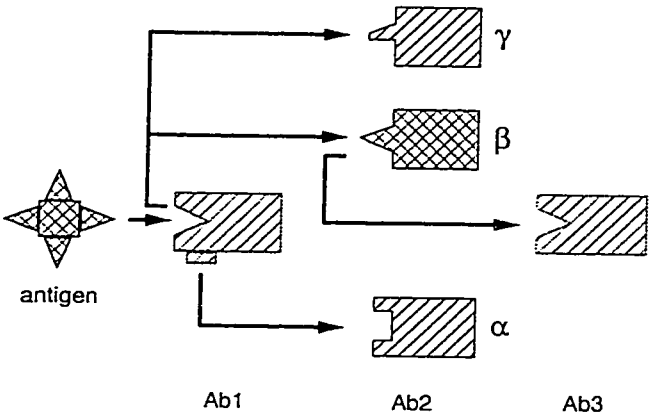

Figure 6: Portion of an idiotypic network. Idiotypes (Ab1) can induce the formation of anti-idiotypes (antibody Ab2), which in turn induce the formation of anti-anti-idiotypic antibodies (Ab3) leading to the formation of the idiotypic network. Sometimes Ab2 can mimic antigen (Ab2β) and can be used as a vaccine.

antibodies in the development of novel therapeutic agents. In many cases antibody-based vaccines are difficult to make due to the difficulties involved in purifying the antigen, obtaining it in sufficient amounts, or low immunogenicity. This is often the case with many carbohydrate antigens. To overcome such limitations it is possible to induce production of an antibody (Ab1, called the idiotype) against the antigen. Ab1 is then used to induce the formation of an anti-antibody (Ab2, anti-idiotype) which is specific to one of the epitopes expressed on Ab1. Three types of Ab2 are possible: α, β, γ. Type Ab2α binds Ab1 away from the Ag binding site. Type Ab2γ binds Ab1 at the Ag binding site, but does not interact with the Ab1 in the same way as the Ag. Type Ab2β binds Ab1 at

the binding site, and will induce the formation of a population of antibodies (Ab3, anti-antidiotype) which are homologous to Ab1. Ab2β therefore functionally mimics the original antigen, and is said to carry an "internal image" of the antigen. The use of a protein (Ab2β) vaccine overcomes the problems associated with the natural antigen, while inducing immunity to the antigen.

1.2 Crystal Structure Analysis

Determination of the structure of the antibodies (R24 and chR24) and the antigen is achieved by analysis of the crystal structure of the proteins. The crystal structure allows us to elucidate the positions of individual atoms of the proteins and carbohydrates, thus giving the molecular structure of the antibodies. Based on these structures, it can be possible to determine how antibodies interact with their antigens, and how some antigens can mimic others.

1.2.1 Lattices, Planes and Indices

Crystal structures, whether inorganic or organic, element or molecular, have a tendency to form distinct, and usually easily identifiable external structures. This initial and simple observation suggested that crystals were themselves arranged from discrete units arrayed in a regular pattern in three dimensions, a proposal which was first postulated by Hauy in 1784 (Woolfson, 1970) based on the cleavage of calcite crystals. A crystal is composed of a repeating array of simple unit cells, which can be described in terms of the volume defined by the intersections of equidistant planes of a coordinate axis system (Figure 7). The surroundings of each such intersection, called a lattice point, are identical. Every unit cell will have the same volume and surroundings as all other cells

defined by the axis system. The lengths of the unit cell along the x, y and z axes are called *a*, *b* and *c*, and in X-ray crystallography the *a*, *b*, and *c* designations are frequently used to refer to the axes. Angles between the axes are termed α, β and γ.

1.2.2 Diffraction of X-rays

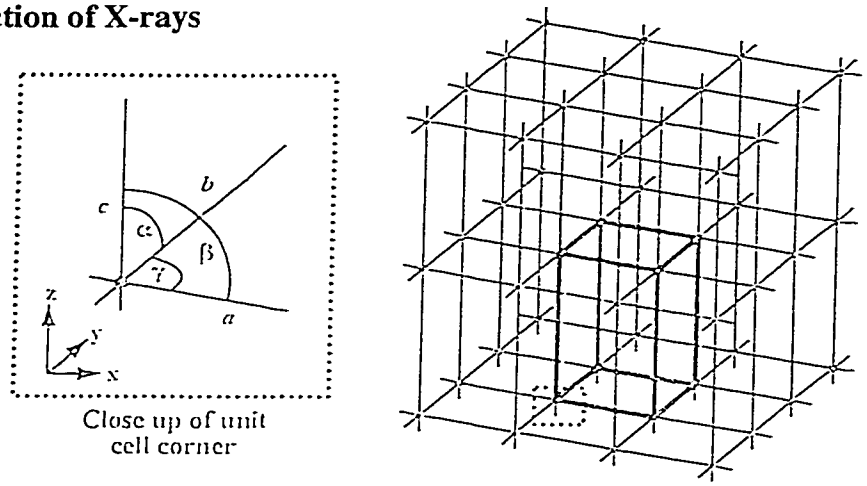

Figure 7: The crystal unit cell. All crystals are made up of a regular repeating three dimensional array of single units. These units, called unit cells, are defined as three dimensional parallel-pipeds defined by sequential parallel x, y and z planes. The length of the cells along these planes is a, b and c, respectively. Angles between ab, bc and ac planes are named α, β and γ

Electromagnetic radiation, such as X-rays, undergoes scattering or diffraction when it interacts with matter. In X-ray diffraction crystallography, this scattering occurs when incident radiation interacts with the electrons around atoms in the protein making up the target crystal and is then propagated in all directions (Figure 8). This scattered radiation undergoes constructive and destructive interference, creating a diffraction pattern which depends on the size and shape of the unit cell and the position of the atoms in the protein molecules.

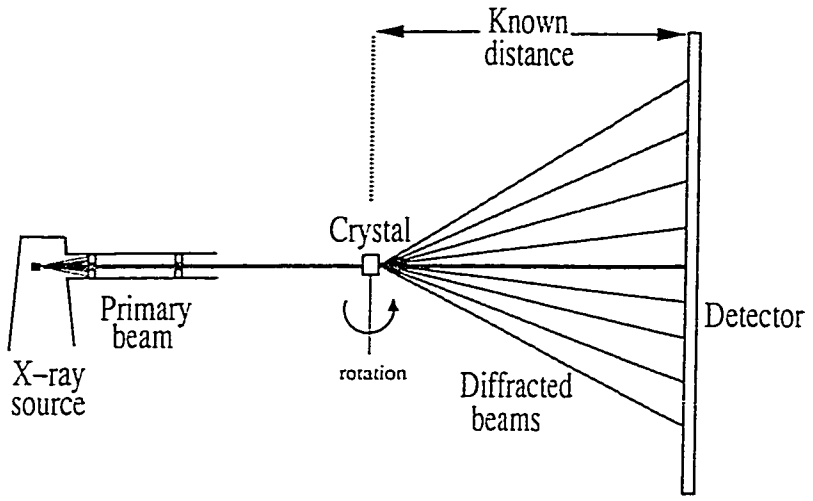

Figure 8: X-ray interaction with crystals. X-rays bombard the crystal, with most of the radiation passing straight through. Some of the X-ray beam is diffracted by the crystal, forming a pattern collected on film or an electronic detector. From this pattern the crystal structure can be elucidated.

The diffraction of X-rays from a crystal was described in mathematical terms by W. L. Bragg as the reflection of radiation from planes which make up the crystal lattice (Stout & Jensen, 1989). Figure 9 shows a schematic of this interaction simplified to two parallel X-ray photons interacting with two parallel planes of the crystal. The radiation

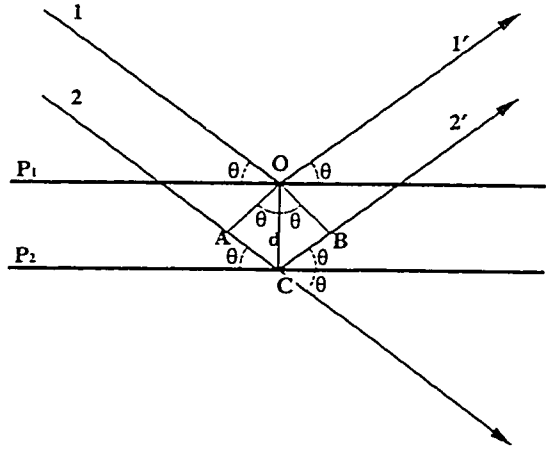

Figure 9: Bragg's Law. The interaction of two parallel incident photons with two parallel crystal planes shows the conditions which are required for constructive interference to take place, leading to the formation of a diffraction pattern.

represented by 1' will be in phase with the reflected ray 2' only if the difference in path length AC+CB (or 2AC) equals an integral multiple of the wavelength, thus defining the conditions necessary for diffraction. This can be expressed as:

$$2AC = n\lambda \qquad \text{Equation 1}$$

or simplified based on the definition $AC = d\sin\theta$ to:

$$2d\sin\theta = n\lambda \qquad \text{Equation 2}$$

known as Bragg's Law. Bragg's Law allows the determination of the parameters of the unit cell from the diffraction pattern, since the position of each diffraction spot is related to a specific set of planes in the crystal. The three properties of each diffracted beam are the amplitude, which is the intensity of the spot, the wavelength, set by the source, and the phase, which cannot be measured. The phase determination process is discussed in section 1.3.2

1.2.3 Symmetry of crystals and unit cells

As mentioned in section 1.2.1 the basis of crystal classification are the seven crystal systems. The crystal unit cell is defined by six parameters, three axial lengths and 3 inter-axial angles. The different degrees of symmetry possible for these parameters define each crystal system. The triclinic system is the most basic system, with symmetry increasing in the next six systems (Table 1.2).

Table 1.2 Crystal Systems and Protein Space Groups (Woolfson, 1970)

Crystal System	Class	Space Groups	Unit Cell Length Restriction	Angle Restriction
Triclinic	1	$P1$	NONE	NONE
Monoclinic (2-fold parallel to b)	2	$P2$, $P2_1$, $C2$	NONE	$\alpha=\gamma=90$
Orthorhombic	222	$P222$, $P2_12_12$, $P222_1$, $P2_12_12_1$, $C222$, $C222_1$, $F222$, $I222$, $I2_12_12_1$	NONE	$\alpha=\beta=\gamma=90$
Tetragonal (4-fold parallel to c)	4 422	$P4$, $P4_1$, $P4_3$, $P4_2$, $I4$, $I4_1$ $P422$, $P42_12$, $P4_122$, $P4_322$, $P4_12_12$, $P4_32_12$, $P4_222$, $P4_22_12$, $I422$, $I4_122$	$a=b$	$\alpha=\beta=\gamma=90$
Trigonal (3-fold parallel to c)	3 32	$P3$, $P3_1$, $P3_2$, $R3$ $P312$, $P321$, $P3_121$, $P3_221$, $P3_112$, $P3_212$, $R32$	$a=b$ $a=b=c$ (R)	$\alpha=\gamma=90$, $\beta=120$ $\alpha=\beta=\gamma<120$
Hexagonal (6-fold parallel to c)	6 622	$P6$, $P6_1$, $P6_2$, $P3_3$, $P6_4$, $P6_5$ $P622$, $P6_122$, $P6_522$, $P6_222$, $P6_422$, $P6_322$	$a=b$	$\alpha=\gamma=90$, $\beta=120$
Cubic	23 432	$P23$, $F23$, $I23$, $P2_13$, $I2_13$ $P432$, $P4_132$, $P4_332$, $P4_232$, $F432$, $F4_132$, $I432$, $I4_132$	$a=b=c$	$\alpha=\beta=\gamma=90$

These seven crystal classes are related to 14 distinct lattice types, called Bravais lattices (Figure 10) (Woolfson, 1970). When combined with all possible internal symmetry elements gives 230 mathematically possible combinations called "space groups" which are listed in the International Tables for X-ray Crystallography, Volume A (Hahn (Ed.), 1989) Of these 230 space groups only 65 contain exclusively chiral symmetry elements, and are therefore applicable to protein structures with their chiral amino acids. Each unit

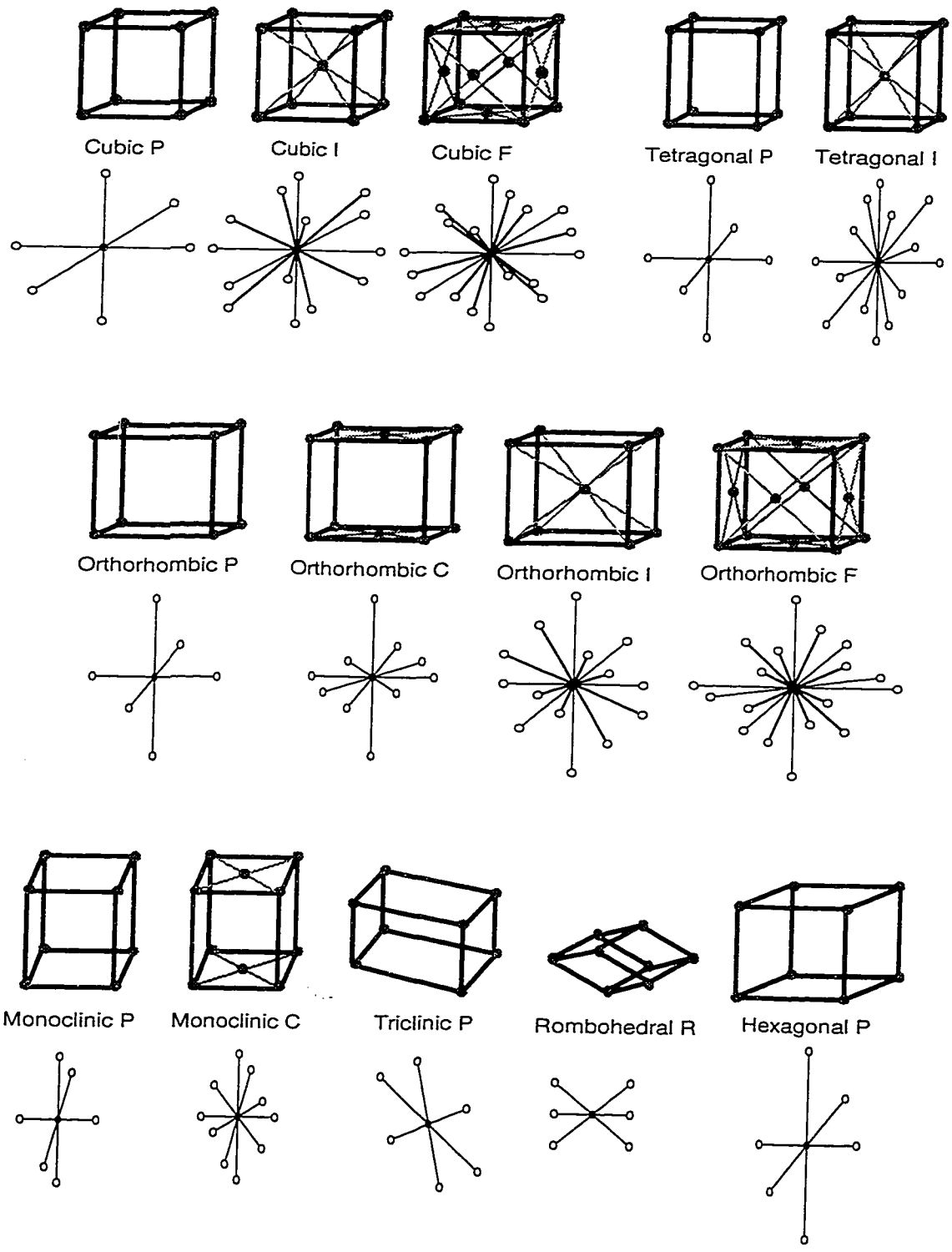

Figure 10: Bravais lattices. These lattices are a combination of the seven crystal systems and the internal symmetry allowed for crystals.

cell is composed of one or more asymmetric units, which is the unique portion of the unit cell (McRee, 1993). It is possible to have more than one molecule per asymmetric unit.

The two space groups pertinent to the research of R24 and chR24 presented in this thesis are $P2_1$ and $C2$. Both of these cells are monoclinic, having one axis of symmetry. $P2_1$ is a primitive unit cell, with a single lattice point per unit cell. In non-primitive cells, more than one such point can exist. The $P2_1$ cell contains two asymmetric units in the unit cell, and the asymmetric units are related to each other by a two-fold screw axis which rotates 180° with a translation of ½ unit cell along the *b*-axis. $C2$ is a non-primitive cell with a lattice point assigned to the C face (*ab* plane) (a point defined by the translation vector ½*a*, ½*b*) and has four asymmetric units per unit cell. The space group $C2$ contains both two-fold rotation and two-fold screw-axes.

1.3 Structure solution

1.3.1 Data collection and resolution

Before solution of the structure begins it is necessary to understand what is meant by resolution. Resolution, given in Ångstroms (1Å = 10^{-10}m), is a measure of the minimum distance at which two adjacent points (atoms within the electron density) are observed as distinct. This minimum separation varies inversely with *d*; therefore high resolution is obtained at low Ångstrom numbers, while low resolution obtained at high Ångstrom numbers. In general, a resolution of 2.5 Å or better allows the determination of main chain and side chain positions, while a resolution of 3.5 Å or worse allows only for the determination of general outline of the main chain and major secondary structures.

The diffraction pattern is collected either on film or by electronic means on a

photo-sensitive detector (such as a charge-coupled device, CCD). In order to obtain all of the possible diffraction spots the crystal is rotated in small increments during data collection, giving three-dimensional information describing the electron density of the molecule. The solution of the structure of a crystallized protein is based on the position of the electron clouds. The shape and density of these clouds define the area of space taken up by the atoms which make up the protein molecule. It is possible to fit the known protein sequence into this electron density, thus solving the three-dimensional arrangement of the protein.

1.3.2 Rotation and translation searches

It is not possible to determine the exact three-dimensional structure of a protein in a crystal directly from the diffraction pattern due to the loss of phase data during the diffraction experiment. Phase information from proteins of completely unknown structure is derived using so-called "heavy atom methods". However, it is possible to solve the phase problem of proteins with analogues of known structure by using the technique of "molecular replacement", where the known structure is used to determine the position and orientation of the molecule within the unit cell. The model structure is first used in a "rotation search" in three dimensions, which compares the diffraction patterns of the known and unknown structures, to give the orientation, followed by a "translation search" in to give the final position within the unit cell. The phases of the model structure in this new position and orientation are used to approximate the phases of the experimental structure. The structure factor (F) is proportional to the square root of the intensity of the scattered X-ray reflection. As the positions of the atoms in the

structure are refined, the results of the observed structure factors (Fo) are compared to the calculated structure factors (Fc) giving a degree of closeness called the crystallographic R-factor:

$$R_{crystallographic} = \frac{\sum_{hkl} |Fo - Fc|}{\sum_{hkl} |Fo|} \qquad \text{Equation 3}$$

The R-factor typically converges to between 15 and 20% in a successfully refined protein structure. The isotropic temperature factors (B) for each atom are also allowed to vary in the refinement process, and are a measure of the motion and vibration of atoms due to thermal effects and slight differences from one unit cell to another. The value of B can be related to the motion of individual atoms, or as an overall value for the molecule, by the equation (Stout and Jensen, 1989):

$$B = 8\pi^2(\bar{u})^2 \qquad \text{Equation 4}$$

where $\bar{u}$ = mean thermal displacement expressed in Ångstroms.

In molecular replacement methods the orientation of the trial structure with respect to the unit cell is specified by a set of angles, called Euler angles, used for the calculation (Figure 11) (McRee, 1993). The trial structure is rotated so that at each increment of k ($\Delta\kappa$), the molecule is moved through both the ϕ and ψ angles at regular increments ($\Delta\phi$, $\Delta\psi$, where the change is usually between 2 and 5°). The correlation

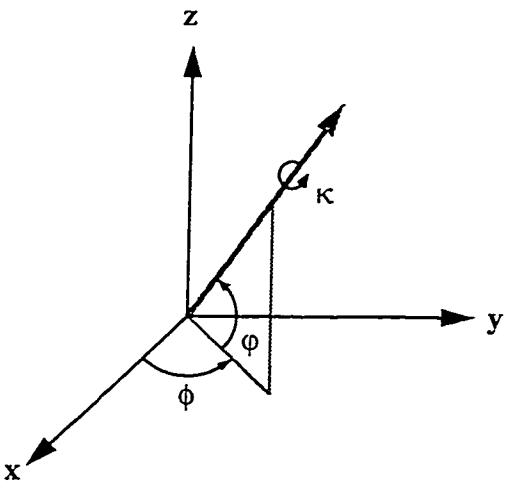

Figure 11: Euler Angles. Schematic of the Euler angles used for rotational searches of molecular position within the crystal.

between the real and calculated diffraction patterns is determined and kept for reference (McRee, 1993). A search over all of the possible angle combinations usually yield only a few good matches between the model and experimental structures. Large correlations will be seen when the orientations of the experimental and model structures coincide.

The translation search is relatively simple, with the position of the molecule simply defined as the relative offsets of the model along each of the three crystal axes. Once the rotation and translation searches have been performed it is necessary to determine if the solution obtained is consistent with crystal symmetry by insuring that no

overlapping of symmetry-related molecules occurs.

1.3.3 Structure refinement

Once the correct molecular replacement solution has been found it is possible to start refining the experimental structure. This is done in three steps

1) "mutation", "insertion" and "deletion" of residues in the model to obtain the amino acid sequence of the experimental protein.
2) calculation of the electron density surrounding the atoms of the protein, and manual fitting the model into observed electron density
3) computer refinement of the structure to maximize the number of atoms in this density, with correct inter-residue angles.

The generation of electron density maps is accomplished via a Fourier transform, using the amplitudes of the observed data and phase of the model data. These maps are based on Fo and Fc which are generated as follows (Amoros and Amoros, 1963):

$$\rho(xyz)=\frac{1}{V}\sum_{h}\sum_{k}\sum_{l}F_{hkl}e^{-2\pi i(hx-ky-lz)} \qquad \text{Equation 5}$$

$\rho(xyz)$ = electron density at the point (x,y,z)
x,y,z = coordinates in three-dimensional space
V = unit cell volume
F = structure factor (intensity + phase information) for reflection (hkl)
h,k,l = Miller indices of each reflection
I = square root of -1

The X-PLOR program, can give several different types of density maps: Fo, Fo-Fc, 2Fo-Fc, 3Fo-2Fc, and omit maps (Brünger, 1992), which provide different information about the comparison of observed and calculated electron density in the X-

ray data. The Fo map is based on the model phases, and the observed diffraction amplitude, and shows the electron density of the observed data. The basic difference map (Fo-Fc) gives the densities of structures present in the observed structure which have no complementary points in the model. This map can be used to determine the location of water molecules around the protein, and the presence of ligands. The 2Fo-Fc and 3Fo-2Fc maps contain information from both the observed and calculated maps, the result being a map with information of the protein density, and how the protein should be fitted into the density. Omit maps allow for the specification of which atoms of a molecule will be used in the map calculation. This is useful in situations where portions of the molecule gave poor diffraction, making the fitting for this section difficult due to lack of data. In the omit map, the section with poor or non-existent electron density is not included in the map calculation, which is instead calculated based on the remaining data, which means that the more correct the fit of the included data, the better the electron density will be for the omitted section (McRee, 1993).

As the structure is fitted into the density it is possible to increase the resolution after several refinement cycles, this means that as the fit of the protein is improved, it is possible to recalculate the map to a higher resolution. The initial fitting is done at lower resolution and is usually limited to the global shape and secondary structure.

The fitting of the model structure within the observed electron density maps is performed with computer programs such as FRODO (Jones, 1978) and SETOR (Evans, 1983), which generate a visual model of the protein chain and the density. The main and side chains are manually fitted into the densities, in a time consuming process which

includes the limitations placed on atom position by bond lengths, allowable peptide angles, and other stereochemical factors. The side chains are generally fit into the electron density by adjusting the side chain dihedral angles after the main chain position has been established (Figure 12).

Following the general placement of the main chain and side chain atoms it is necessary to perform a positional refinement. The positional refinement incorporates all the factors of geometry, and applies them to the molecule. The result is a minimization of the differences between experimental and observed positions, which is concurrently minimized for the deviation of the model atom from a mathematically ideal geometry, by moving the coordinates to the new, more correct positions (Brünger, 1992, McRee, 1993). The X-PLOR program performs several cycles of this positional refinement, evaluating the overall fit and geometry of the structure during each cycle, then reapplying the positional refinement to the new coordinates. Repetition of these cycles should lead to a

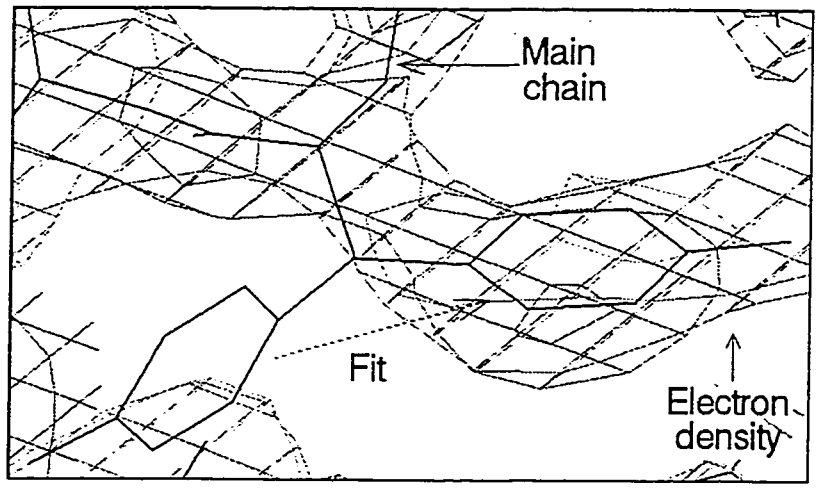

Figure 12: Positioning of atoms within the electron density cloud. The atoms which form amino-acid side chains are rotated about the interatomic bonds in order to place them in the correct position within the electron densities while preserving stereochemistry.

convergence in the differences between the model and experimental data sets leading to a convergence in the R-factor (McRee, 1993).

1.4 Structural Data

Solution of the protein structure is not in itself the end of research. Information on the coordinates of the protein atoms makes possible an analysis of the secondary and tertiary structures and how these influence the activity and function of the protein. The solved structure allows the viewing of the three-dimensional structure of the protein using molecular graphics computer programs such as SETOR and GRASP (Nicholls, 1991). This allows for the visualization of any major structures of the protein, such as binding sites, folding patterns, and inter- and intra-molecular interactions. The visual representation of the solvent accessible surface of the protein allows for the modelling of protein-ligand and protein-protein interactions, and can lead to an improved understanding of these interactions.

1.5 Binding Studies

The comparison of murine and chimeric antibodies by X-ray crystallography allows for the determination of structural differences brought on by the humanization process, which can be then correlated with the observed *in vivo* and *in vitro* activity of each antibody group. Interactions between antibodies and antigens, and between antibodies can be assessed by Enzyme-Linked Immunosorbent Assay (ELISA) (Goding, 1983), which provides information on the binding avidity of an antibody to a molecule which is linked to the surface of a plastic dish.

Real-time studies of immunoglobulin-antigen interactions can be carried out by

surface plasmon resonance (SPR). The SPR experiment uses the BIAcore® system. Either the antibody or antigen is anchored in some way to the surface of a gold-plated sensor chip, with an appropriate ligand allowed to pass over this surface in a buffer system (Figure 13). Measurements of the ligand binding on (k_{on}) and off (k_{off}) rates are made based on changes in surface optical properties due to surface plasmon resonance giving a response *vs* time sensogram (Karlsson et al., 1991). The kinetic association (k_a) and dissociation (k_d) rate constants are calculated from mathematical interpretation of the sensogram. Comparison of SPR and ELISA data with the structural information gained from X-ray crystallography allows for an analysis of how and why these differences in structure effect the activity of the antibodies.

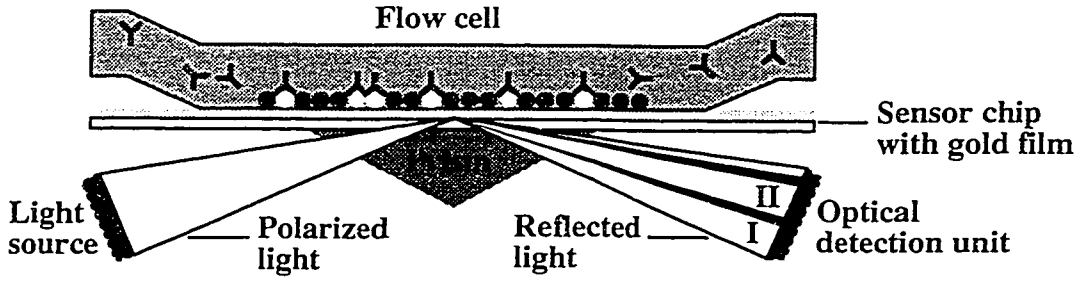

Figure 13: BIAcore® surface plasmon resonance.
The binding of molecules to the sensor chip surface, and the subsequent interactions of other molecules with the first group can be measured in real-time by the change in wavelength of polarized light reflected off of the sensor chip.

2 MATERIALS AND METHODS

2.1 Equipment and reagents

The analytical grade reagents Zinc Sulfate, Sodium Cacodylate, Polyethylene Glycol (PEG) 800, PEG 1000, Sodium Acetate, Imidazole, Sodium Formate, Ethanol, Methanol, Sodium Azide, Beta-Mercaptoethanol, Trichloroacetic Acid, MES, Sodium Chloride, and Mercury-Papain were purchased from Sigma-Aldrich Canada Ltd. Oakville, ON or its subsidiaries. Analytical grade Zinc Acetate and Hydrochloric acid were purchased from AnalR. TRIS-HCl was obtained from Anachemia, Mississauga, ON. Cupric Sulfate came from BDH, Toronto, ON. Silver Stain Oxidizer, Reagent, and Developing fluid were purchased from Bio-Rad laboratories (Canada) Ltd., Mississauga, ON as were Protein A resin, Binding and Elution Buffers (MAPS II kit). Prepared sparse matrix crystallization screening kits: Crystal Screen I (CS I) and Crystal Screen II (CS II) were purchased from Hampton Research, Laguna Hills, CA, USA. Plastic coverslips were purchased from VWR Scientific (Canada), well seals were performed with DOW Corning Compound 111. Phast system, IEF and SDS-PAGE gels, coomasie stain, and Sephadex G-25 column were purchased from Pharmacia Biochemica Canada Ltd, Baie d'Urfe, PQ. BIAcore® sensor system and reagents were made by Pharmacia Biosensor AB, Uppsala, Sweden. The Gilson series 800 HPLC unit used for separation of Fab from digest mixture was purchased from Gilson Scientific Canada, Inc. a subsidiary of VWR Canada, Inc. The ion exchange resin HPLC column Shodex CM825 was purchased from Phenomenex, Torrance, CA, USA. Centricon-10 concentrators were purchased from Amicon, Inc., Beverly, Massachussets, USA. Low Temperature Upright Incubator was

purchased from VWR Scientific (Canada).

2.2 Antibody cell lines and antibody purification

Murine anti-GD3 monoclonal antibody R24 (IgG3) and BEC2 anti-idiotypic antibody (IgG2a) were obtained in ascites form from Dr. Paul B. Chapman, Sloan-Kettering Cancer Research Centre, New York, NY, USA. Mouse-human chimeric R24 (chR24) consists of R24 heavy and light variable region genes ligated to the gene sequence coding for human IgG1(κ) and was provided by Dr. Alan Jarvis (Repligen Corporation, Cambridge, MA).

BEC2 and R24 antibodies were affinity-purified from ascites using Protein A column chromatography. Fab fragments were prepared from the purified antibodies by digestion with papain (Yamaguchi, 1994). Mercuripapain was activated by β-mercaptoethanol (βME) in a molar ratio of papain : βME = 1:25, the mixture diluted to 100 mL with 20 mM NaOAc pH 5.4. The βME and HgβME were separated from the activated papain on a Sephadex G-25 Medium column and eluted using 20 mM NaOAc pH 5.4. Elution fractions were assayed for protein content by U.V. spectrometry (280 nm wavelength); where $A_{280}/2.5$ equals the papain concentration in mg/mL. The digest mixture was prepared with IgG, papain (1:200 papain:IgG molar ratio) (Equation 6), and

$$V_{papain} = \frac{[Ab](V_{Ab})}{[papain](200)} \qquad \text{Equation 6}$$

carried out in the presence of DTT (8:1 DTT:IgG molar ratio); and brought to final volume with 20 mM NaOAc pH 5.4 at 25 C. The digest reactions were quenched with

moles iodoacetamide : DTT = 2.2. Time trial results established optimal digests at 3.5 hrs for R24, 2.5 hrs for chR24 and 3.5 hrs for BEC2. The quenched digests were dialysed overnight against 20 mM NaOAc pH 5.4. Dialysed digest was filtered on a 0.22 µm low protein-binding filter and degassed under vacuum in preparation for HPLC purification. The resultant Fab fragments were purified on a carboxymethyl HPLC column with buffer A: 20 mM NaOAc pH 5.4 and buffer B: 20 mM NaOAc pH 5.4, 2 M NaCl. The run conditions, including run time, NaCl concentration gradient, and maximum salt concentration were altered to optimize peak separation. Protein content was assayed by absorption at 280 nm wavelength, with the main peak and minor peaks assayed by SDS-PAGE (12.5% acrylamide gel), and IEF PAGE (3-10 pI range gel). Fab peaks were pooled and spin- concentrated to between 8 and 12 mg/mL (determined by UV spectrometry at 280 nm wavelength) in Amicon Centricon-10 concentrators. Sodium azide was added to a final concentration of 0.02% (v/v). Concentrated Fab samples were kept at 4°C prior to crystallization trials.

2.3 R24 and BEC2 Binding studies

Experiments were performed by Dr. C. Roger Mackenzie and Tomoko Hirama (IBS-NRC, Sussex Drive, Ottawa, ON), to purify BEC2 Fab specific to R24, to purify the R24-BEC2 complex, and to measure the affinity of the R24-GD3, chR24-GD3, R24-R24 and BEC2-R24 interactions. The first experiment was performed by binding R24 IgG to the Protein A column, and then applying BEC2 Fab fractions to the R24-Protein A matrix. In the second experiment BEC2 Fab and R24 Fab were mixed in a 1.27:1 molar ratio, then separated by size exclusion on a Superdex 75 column under FPLC conditions,

using Pharmacia FPLC pump system, and LKB HPLC pump system (IBS-NRC, Sussex Drive, Ottawa, ON). The runs were carried out in 10 mM HEPES (pH 7.4), 150 mM NaCl and 3.44 mM EDTA. Measurement of antibody-antigen, homophilic and idiotype-anti-idiotype binding interactions (affinity) was carried out using the BIAcore® system, in the same buffer system as the size exclusion chromatography. R24 and chR24 interactions with GD3 were measured by binding of these IgG and Fab to GD3-bearing liposomes cross-linked to the sensor chip. R24 homophilic binding was carried out by letting free R24 IgG flow over a sensor chip with cross-linked R24 IgG. R24-BEC2 interactions were measured by using a sensor chip with bound R24 and flowing BEC2 over this surface. Kinetic measurements of the association (k_a) and dissociation (k_d) rate constants were made and the K_D calculated based on these results.

2.4 Crystallization

Primary determination of crystallization conditions was carried out using a sparse matrix approach with CS I and CS II (Carter, and Carter, 1979; Jancarik and Kim, 1991), and with duplicate CS I solutions made in our lab. Premade CS I and CS II solutions come ready-to-use; the duplicate CS I was prepared using analytical grade reagents from Fluka Biochemica (division of Sigma-Aldrich), with each component filtered separately with 22 micron nylon filters, prior to mixing, based on Hampton Research specifications. These two sets consist of premixed solutions (50 and 48, respectively) of buffers, inorganic salts and precipitants in a variety of combinations. This allows the methodical study of a wide range of variables which alter sample-sample and sample-solvent interactions, slightly biased for conditions most often seen in literature reports of

successful crystallization conditions. This technique also provides solubility information, even if the crystallization is less than successful. 1 µL of Fab concentrate was mixed with 1 µL of reservoir buffer and the resultant drop suspended on a plastic coverslip over 1 mL of the reservoir buffer in a Linbro tissue culture 24 well plate in a hanging drop experiment (McPherson, 1985) (Figure 14). Drops were evaluated for crystal growth daily for the first week, and weekly after the initial period.

Refinement conditions were altered by changing pH, counter ions, and the amount

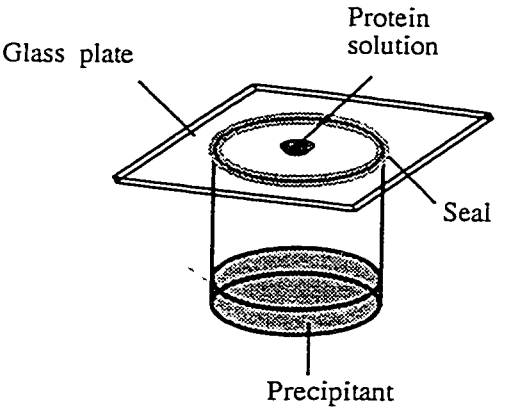

Figure 14: Hanging drop experiment A 2 µL drop of protein-crystallization buffer is placed on a plastic coverslip, which is then inverted and placed over a Linbro plate well filled with 1 mL crystallization buffer. The seal is made with a silicone grease.

of and type of PEG in the crystallization buffer (Table 2.1 and 2.2). Refinement hanging drop size increased to 4.0 and 6.0 µL with the Fab:mother liquor ratio 1:1 and 1:3 respectively. The concentration of R24 Fab was increased from 6 mg/mL in the first refinement drops to 8 mg/mL in the second refinement drops. The chR24 Fab was increased from 8-10 mg/mL in the first refinement to 12-15 mg/mL in the second refinement. 20°C crystallizations were performed in the incubator, 4°C crystallizations were performed in a cold room. Refinement solutions for R24 were prepared as in Table

2.1, refinement solutions for chR24 were prepared as in Table 2.2.

Table 2.1: R24 Fab refinement conditions.

Refinement Set (original solution)	pH range*	Precipitant	Precipitant Concentration	Buffer	Salt	Drop Size
1 (CS I #25)	6 - 7	Na Acetate	0.5, 1.0, 2.0, 3.0 M	Imidazole	-	4 and 6 mL
2 (CS I #33)	6 - 8.5	Na Formate	1.0, 2.0, 3.0, 4.0 M	-	-	4 mL
3 (CS I #36)	8-9	PEG 8000	8, 10, 13%	Tris HCl	-	4 mL
4 (CS 1I #45)	6 - 8.5	PEG 8000	13, 18, 23 %	Sodium Cacodylate	Zinc Acetate	4 and 6 mL

* in 0.5 unit increments. Equilibration of the hanging drop conditions took place at 20°C and 4°C.

Table 2.2: chR24 Fab refinement conditions.

Refinement Set (CS I #45)	pH range (0.5 unit increments)	PEG (MW)	PEG Concentration	Drop Size
1	6 - 8.5	8000	13, 18, 23 %	4 and 6 mL
2	6 - 8.5	8000	13, 18, 23 %	4 mL
3	6 - 8.5	10000	13, 18, 23 %	4 mL

Equilibration of the hanging drop conditions took place at 20°C and 4°C, and in the presence of two different zinc salts; Zinc Sulphate, and Zinc Acetate.

Both micro and macro seeding were carried out with R24 and chR24 refinement sets. Microseeding was performed by crushing small regular and larger multimeric crystals, then dipping a wand tipped with a single human eyebrow hair, cleaned with ethanol, into the resulting micro crystal-mother liquor mixture. The wand was then inserted perpendicularly to the drop surface into pre-equilibrated (24 hrs) drops prepared according to the refinement conditions and drawn across the drop. Macroseeding was carried out by taking single small regular crystals and placing them whole into pre-equilibrated hanging drops.

2.5 X-ray diffraction experiment

Data collection was carried out at Queens University, Kingston, Ontario, Canada for chR24 and at the Cornell High Energy Synchrotron Source (CHESS) at Cornell University, Ithaca, New York, USA for R24 and chR24 with ligands. Crystals prepared for data collection at Queens University were placed in 0.4 mm diameter glass capillaries (one crystal per capillary), with a small amount of the mother liquor to maintain hydration. These capillaries were then capped with sealing wax and embedded in plasticine for transport. Data were collected at room temperature with a Mar 30 cm image plate detector mounted on a rotating anode RU600 X-ray generator. Cornell University has a low temperature setup for data collection. In this protocol whole single crystals are placed in small nylon loops, by "fishing" the crystal out of the crystallization drop. The crystal and loop are then dipped in a cryopreserving solution (mother liquor with 25-30% glycerol, which replaces the solution around the crystal, and immediately transferred to the camera spindle which is bathed in a constant stream of N_2 gas at -189 °C. The data collection proceeds under low temperature using synchrotoron radiation and the Princeton University 1k CCD detector.

Lorentz-polarized corrected intensities were obtained using the program DENZO (Otwinowski and Minor, 1993).

Determination of the chR24 structure was based on the R24 model, previously solved to 3.2 Å, and molecular replacement methods were performed using the program X-PLOR (Brünger, 1992). The orientation and position of the variable domain of chR24, which is identical in sequence to the R24 Fv, was found using X-PLOR search function.

The position of the chR24 constant domains (C_L and C_{H1}) was determined using Patterson Correlation (PC) refinement function in tandem with an elbow-angle search in XPLOR. Once the position of the constant domains was found the sequence of these R24 model structures was modified, using SETOR, to match human IgG (κ). The modified structure was then put through a series of Hendrickson-Konnert refinements of simulated slow-cool annealing with manual refitting of individual residues into the omit maps after each cycle. Once the R_{factor} value was brought to approximately 0.18, water molecules were positioned around the Fab molecule. The choice of position for water molecules was done manually by searching for regions of high electron density in the difference map (Fo-Fc) generated by XPLOR.

The solvent accessible surface of the antibodies was calculated using the program ms (Connolly, 1983), with computer modelling of the surface performed using SETOR. SETOR was also used for the modelling of the terminal sialic acid residues of GD3, for the determination of the possible antigen-antibody interactions, and for modelling of the BEC2 epitope and its possible interactions with R24 and chR24.

ChR24-ligand structure was solved based on the chR24 structure. The correct rotation was first determined, followed by positional refinement. The putative position of the ligand was then examined, with the program FRODO, for regions of high electron density using 3Fo-2Fc maps generated by XPLOR.

3 RESULTS:

3.1 Purification and Crystallization

3.1.1 R24

R24 IgG ascites was purified according to described protocols using protein A, and cleaved to Fab and Fc by proteolytic digestion. HPLC cation exchange purification gave a symmetric main peak, followed by a distinct small peak (Figure 15a). Analysis of the two peaks by SDS and IEF PAGE showed the major peak to be Fab (Figure 15a). The Fab fraction was concentrated to between 3 and 6 mg/mL, with higher concentrations showing large losses due to precipitation of the Fab. The primary crystallization trials were carried out using the sparse matrix crystallization screening kits CS I and CS II described in section 2.1. CS II gave no crystals after an eight month period. Two weeks after the initial formation of CS I hanging drops, small crystals could be seen in three wells (33, 36, 45) with crystals forming in well 25 a week later. After seven weeks only these four wells showed crystals, and growth levelled off, with no increase in size seen over a period of 5 more weeks. The crystals varied in size and morphology; long thin needle and fan structures, plates, and rectangular, with an average size of 0.1×0.05×0.2 mm^3. Consequently these conditions were used for the development of the refinement conditions for further crystallization. The crystals obtained in the first round of refinements (Table 3.1), were too small to be used for data collection. Thus they were used for micro- and macroseeding in the second round of refinement crystallization experiments at 20°C (Table 3.2). The crystallization refinement results are summarized below.

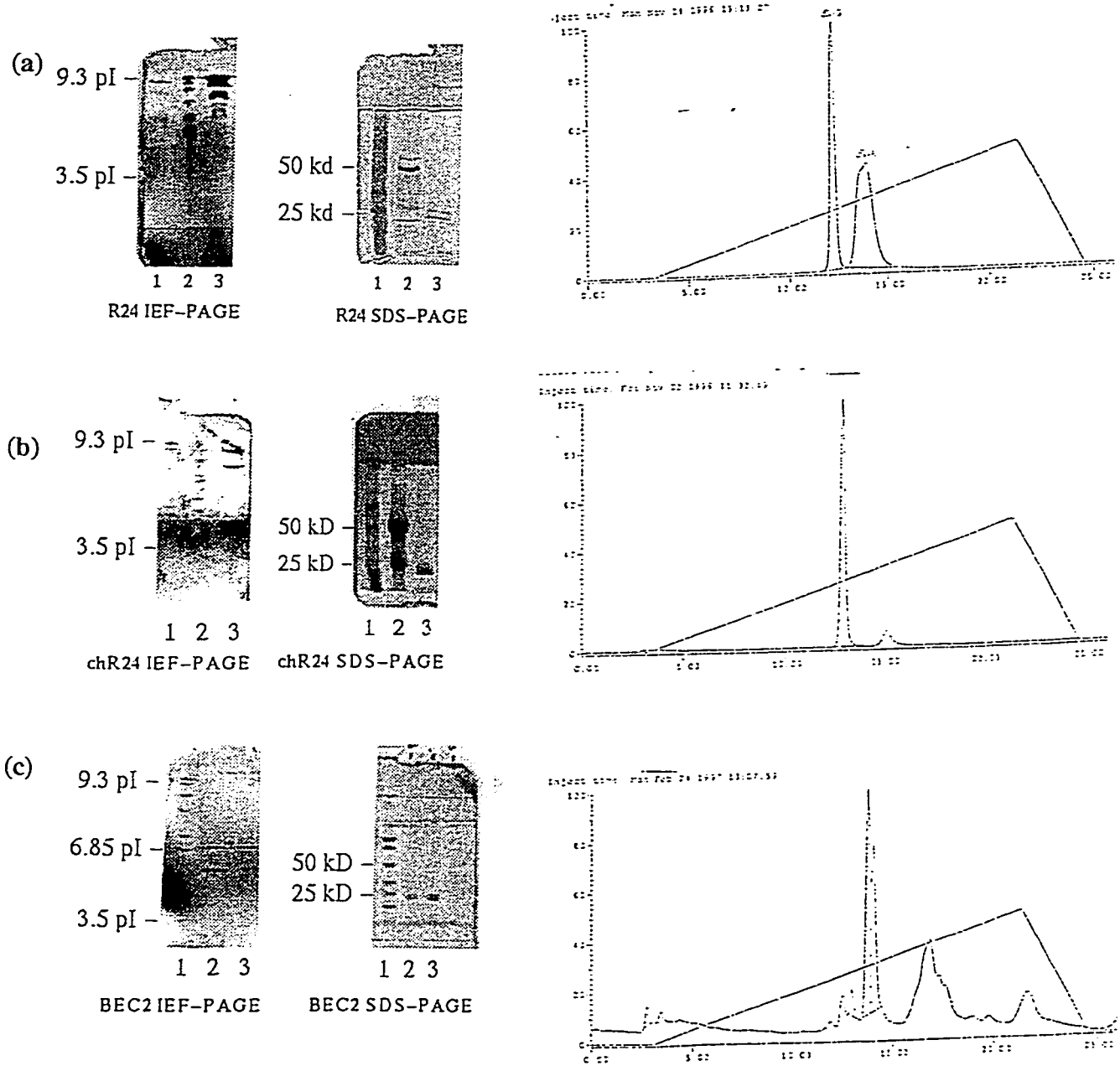

Figure 15: Fab purification results. HPLC, SDS- and IEF-PAGE results are given for the purification of the Fab from the IgG digest. R24(**a**) and chR24(**b**) gave single main peak fractions (Fab) during cation exchange HPLC. BEC2(**c**) showed a double major peak, making purification of Fab difficult. For R24 and chR24 SDS: 1 = Standard, 2 = Fab, 3 = Fab; for IEF 1 = Fab, 2 = Standard, 3 = IgG. For BEC2 SDS and IEF 1 = Standard, 2= major peak 1, 3 = major peak 2. SDS-PAGE was performed under reducing conditions.

Table 3.1: Results for R24 first round refinement crystallization.

Refinement Set (original solution)		1 (CS I #25)	2 (CS I #33)	3 (CS I #36)	4 (CS I #45)
pH range*		6 - 7	6 - 8.5	8 - 9	6 - 8.5
[PEG 8000] in %		13, 18, 23 %	13, 18, 23 %	8, 13, 18%	13, 18, 23 %
Drop Size (mL)		4, 6	4	4	4, 6
20°C trial	Crystal size**	0.05×0.1×0.2	0.05×0.05×0.2	0.1×0.2×0.35	0.1×0.2×0.25
	Use	microseeding	micro and macroseeding	micro and macroseeding	microseeding
4°C trial	Crystal size**	0.05×0.1×0.15	0.05×0.15×0.15	0.1×0.1×0.2	0.1×0.1×0.2
	Use	microseeding	microseeding	microseeding	microseeding

* 0.5 unit increments. **Average size in mm^3.

Table 3.2: Results for R24 second round refinement crystallization.

Refinement Set (original solution)	1 (CS I #25)	2 (CS I #33)	3 (CS I #36)	4 (CS I #45)
pH range*	6 - 7	6 - 8.5	8 - 9	6 - 8.5
[PEG 8000] in %	13, 18, 23 %	13, 18, 23 %	8, 13, 18%	13, 18, 23 %
Drop Size (mL)	4	4	4	4
Crystal size**	0.05×0.1×0.2	0.1×0.25×0.2	0.15×0.2×0.3	0.2×0.2×0.25
Use	not used	data collection	data collection	data collection

* 0.5 unit increments. ** Average size in mm^3.

Twenty of the attempted crystallization refinement conditions yielded crystals, with large variations in shape and morphology. Growth of single crystals was best in macroseeded conditions, and fastest growth was observed in microseeded conditions, with crystals appearing after five days, and growth levelling off at about 4 weeks. Three large crystals (average size 0.25×0.35×0.6 mm^3) were obtained, but these were either multiple or had large inclusions within the crystal. As well, six single crystals were obtained from the second refinement round, with an average size of 0.15×0.15×0.4 mm^3. Data collection was carried out on the single crystals in a low temperature setup at the CHESS facility in

Ithaca, New York, however none of them diffracted beyond 4.0 Å and no data were collected.

3.1.2 BEC2

The anti-idiotypic antibody BEC2 was chosen for crystallization in order to elucidate the structure of the putative R24-binding domain in order to shed light on how a polypeptide can mimic the carbohydrate antigen GD3. The BEC2 Ab was purified using protein A from ascites and digested as per the IgG protocol described in section 2.1, to give Fab and Fc. The purification of BEC2 proved difficult; despite repeated attempts to optimise the HPLC running conditions three major peaks were observed (Figure 15b). The first two peaks were large narrow and symmetric, but overlapped each other. The third peak was broad asymmetric and overlapped three minor peaks. SDS and IEF analysis showed the first two overlapping peaks to be Fab, with the first peak being approximately twice as intense in colour as the second (Figure 15c). The overlapping Fab peaks presented a two fold problem: 1) it was not possible to completely purify either peak, leading to losses in pure Fab fractions; 2) it was not possible to determine which fraction (or both) bound R24. It was attempted to separate the BEC2 Fab fractions by immunospecific means. In order to do so R24 IgG was bound to protein A and the BEC2 Fab were applied to this column. Although a portion of the Fab fraction from both peak 1 and peak 2 bound to R24, it was not possible to purify the resulting complex using FPLC and HPLC methods. In order to avoid missing the correct Fab, both fractions were concentrated to approximately 8 mg/mL and CS I and CS II screens were carried out using both fractions. Over 12 months no crystal growth was seen in any of these

crystallization setups.

3.1.3 R24:BEC2 complex

Co-crystallization of R24 and BEC2 was attempted to obtain structural data on both the BEC2 and the idiotope-anti-idiotope interaction. The difficulty in obtaining a pure BEC2 Fab led to two sets of co-crystallization trials; one set of CS I and CS II solutions for each of the two Fab fractions of BEC2 mixed in a 1.2:1 molar ratio with R24 Fab. Over the course of eight months no crystal formation was observed, suggesting that a stable complex was not forming. Due to a lack of structural data on BEC2 computer modelling of the BEC2 sequence was used to determine the putative R24 binding region.

3.1.4 chR24

The humanized version of murine R24, chR24, was prepared at Sloan-Kettering for clinical trials. The chimer maintains the murine variable domains responsible for GD3 specific action, but has human constant domains to minimize immune response in patients. It was necessary to determine the structure of this chimer in order to determine if the antigen binding epitope remained the same or if it had been affected by the change in the constant domains.

ChR24 was obtained as a purified IgG and subjected to a 2.5 hour papain digest according to the protocol in section 2.2. A large symmetric single peak was obtained on HPLC purification and identified as Fab by SDS and IEF PAGE methods (Figure 15c), with a very minor second peak. The chR24 Fab was concentrated to between 8 and 15 mg/mL, with no losses due to precipitation observed. The broad spectrum approach was

repeated with chR24 using both CS I and CS II solutions for preliminary trials (carried out as per section 2.3). Only solution CS I number 45 produced regular crystals, other solutions yielded precipitates or aggregates. Crystals in solution number 45 appeared after ten days, and continued to grow for approximately five weeks after the initial crystallization setup. The crystals obtained from the initial CS I trial had two distinct morphologies: long narrow thin crystals arranged in a fan-like pattern, and regular, rectangular brick shaped crystals, with an average size of $0.05 \times 0.02 \times 0.5$ mm^3. The refinements were performed in two different salts of zinc. Zinc sulfate yielded only thin multiple fanlike crystals, not suitable for x-ray crystallography, and was not repeated. The results of the zinc acetate series of refinements based on CS I solution 45 are summarized in Table 3.3 and 3.4. The first round of refinements was performed with the chR24 Fab concentration at 10 mg/mL the second round was performed with the concentration of 15 mg/mL. The first refinement crystals were relatively small and with the exception of two wells were used for microseeding of the second set of refinements. The second round of refinements yielded eight single crystals large enough for data collection (average size $0.2 \times 0.25 \times 0.4$ mm^3). The two largest cubic crystals were placed in separate capillary tubes and sealed in preparation for data collection at Queen's University.

Table 3.3: Results of chR24 first round refinement crystallization

Refinement based on CS I #45, with Zinc Acetate as salt						
	20°C			4°C		
Refinement Set	1	2	3	1	2	3
pH range*	6 - 8.5	6 - 8.5	6 - 8.5	6 - 8.5	6 - 8.5	6 - 8.5
PEG (MW)	8000	8000	10,000	8000	8000	10,000
[PEG] in %	13, 18, 23	13, 18, 23	13, 18, 23	13, 18, 23	13, 18, 23	13, 18, 23
Crystal size**	0.1×0.15 ×0.15	0.05×0.15 ×0.25	0.1×0.2×0.2	0.1×0.1×0.1	0.05×0.1 ×0.1	0.1×0.1×0.1
Morphology	flat plate, cubic,	fanlike needles, cubic,	flat plate	cubic	cubic	needles, cubic
Use	micro seeding	micro- and macro seeding	micro seeding	micro seeding	micro and macro seeding	macro seeding

* in 0.5 unit increments. ** average size in mm^3

Table 3.4: Results of chR24 second round refinement crystallization

Refinement based on CS I #45, with Zinc Acetate as salt						
	20°C			4°C		
Refinement Set	1	2	3	1	2	3
pH range*	6 - 8.5	6 - 8.5	6 - 8.5	6 - 8.5	6 - 8.5	6 - 8.5
PEG (MW)	8000	8000	10,000	8000	8000	10,000
[PEG] in %	13, 18, 23	13, 18, 23	13, 18, 23	13, 18, 23	13, 18, 23	13, 18, 23
Crystal size**	0.2×0.2 ×0.3	0.05×0.1 ×0.3	0.2×0.2 ×0.4	0.2×0.2 ×0.2	0.15×0.2 ×0.2	0.1×0.2 ×0.3
Morphology	cubic	needles and cubic	cubic	cubic	cubic	needles and cubic
Use	data collection, soaking with ligand	-	data collection	data collection	-	-

* in 0.5 unit increments. ** average size in mm^3.

The chR24 data collection was successful and is described under data collection.

3.1.5 chR24 and ligands

The investigation of the chR24 structure with its ligands was pursed through both co-crystallization (as described in section 3.1.3), and through crystal soaking. The soaking procedure involved growing crystals of chR24 and subsequently soaking the crystals in a solution of mother liquor and carbohydrate ligand. Two of the crystals obtained in chR24 refinement experiments (second round, see table 3.4) were treated in this way, using NeuAc α2-8 NeuAc as the ligand. Both crystals were prepared for data collection, which was carried out at Queens University, Kingston, Ontario, and the larger of the two crystals ($0.2\times0.25\times0.4$ mm^3) yielded data.

While the BEC2 and the R24:BEC2 complex crystallization experiments were attempted, it was decided that computer modelling methods would be used to determine what sequences of the BEC2 could interact with the GD3 binding site of R24 (discussed fully in section 4.3.2).

The putative binding sequence of BEC2 was found, by Dr. Ross Williams, IBS-NRC, Ottawa, Ontario, to closely resemble that of the Hamburger Pentapeptide (H.P.) (Prenner, 1987). Both the H.P. and the BEC2 peptide sequences were purchased and prepared for co-crystallization trials with chR24. CS I and CS II screens were used for both sets of chR24-ligand samples, and in both cases only well 45 of CS I showed crystal growth. Refinement sets of solution CS I no. 45 were prepared using two different Zinc salts: Zinc Sulfate and Zinc Acetate. The co-crystallization refinement experiments (Zinc Acetate) are summarized in Table 3.5

Table 3.5: Results of chR24-ligand first round refinement co-crystallization

Refinement based on CS I #45, with Zinc Acetate as salt						
	20°C			4°C		
Refinement Set	1	2	3	1	2	3
pH range*	6 - 8.5	6 - 8.5	6 - 8.5	6 - 8.5	6 - 8.5	6 - 8.5
PEG (MW)	8000	8000	10,000	8000	8000	10,000
[PEG] in %	13, 18, 23	13, 18, 23	13, 18, 23	13, 18, 23	13, 18, 23	13, 18, 23
Ligand	Hamburger Pentapeptide					
Crystal size**	0.05×0.1 ×0.1	0.02×0.05 ×0.05	0.02×0.05 ×0.2	0.01×0.02 ×0.02	0.1×0.1 ×0.15	0.05×0.05 ×0.06
Morphology	multiple cubic, cubic	hexagonal, demi-hexagonal	long needles, demi-hexagonal	demi-hexagonal	cubic, hexagonal demi-hexagonal	demi-hexagonal
Use	macro seeding	micro seeding	-	-	macro seeding	micro seeding
Ligand	BEC2 Analogue					
Crystal size**	0.02×0.02 ×0.01	0.02×0.03 ×0.01	0.07×0.07 ×0.1	0.03×0.04 ×0.04	0.03×0.05 ×0.05	0.03×0.03 ×0.03
Morphology	hexagonal, demi-hexagonal	hexagonal	thick hexagonal	cubic, demi-hexagonal	hexagonal	hexagonal, demi-hexagonal
Use	-	-	macro seeding	micro seeding	micro seeding	micro seeding

* in 0.5 unit increments. ** average size in mm^3

All crystals obtained in the Zinc Sulfate refinements were multiple, and narrow, thus not useful for data collection. The Zinc Sulfate refinements were not pursued in the second round. This series gave no crystallization, and was not pursued further. Two wells from the HP series and one well from the BEC2 analogue series were chosen to provide crystals for macroseeding. The co-crystallization in the presence of zinc acetate was repeated for both polypeptide ligands, using the microseeding technique, the results are listed in Table 3.6.

Table 3.6: Second Round of chR24-H.P. and chR24-BEC2 Analogue Co-crystallization Refinements.

Refinement based on CS I #45, with Zinc Acetate as salt						
	20°C			4°C		
Refinement Set	1	2	3	1	2	3
pH range*	6 -8.5	6 -8.5	6 -8.5	6 -8.5	6 -8.5	6 -8.5
PEG (MW)	8000	8000	10,000	8000	8000	10,000
[PEG] in %	13, 18, 23	13, 18, 23	13, 18, 23	13, 18, 23	13, 18, 23	13, 18, 23
Ligand	Hamburger Pentapeptide					
Crystal size**	0.1×0.25 ×0.4	0.1×0.1×0.1	0.2×0.35 ×0.4	0.1×0.1×0.25	0.1×0.1 ×0.15	0.1×0.15 ×0.15
Morphology	hexagonal	hexagonal, demi-hexagonal	hexagonal, demi-hexagonal	hexagonal,	hexagonal, demi-hexagonal	hexagonal, demi-hexagonal
Use	data collection	-	data collection	-	-	-
Ligand	BEC2 Analogue					
Crystal size**	0.2×0.15 ×0.25	0.1×0.25 ×0.35	0.05×0.05 ×0.1	0.15×0.3×0.3	0.02×0.07 ×0.1	0.02×0.02 ×0.08
Morphology	hexagonal, demi-hexagonal	demi-hexagonal	demi-hexagonal	hexagonal, demi-hexagonal	hexagonal, demi-hexagonal	hexagonal, demi-hexagonal
Use	data collection	data collection	-	data collection	-	-

* in 0.5 unit increments. ** average size in mm^3.

Five wells (two H.P., and three H.P. analogue) from the second refinement yielded single crystals (average size 0.1×0.15×0.5 mm^3) however none of these crystals were of good enough quality for X-ray diffraction.

3.2 X-ray diffraction data collection

For the previously solved R24 crystal, 58,762 reflections had been measured yielding 24,672 unique reflections to 3.1 Å resolution with Rsym = 0.075 and 92% completeness. The cell dimensions are a = 139.2, b = 82.1, c = 73.6 Å and $\beta = 94.1°$ in

the monoclinic space group $P2_1$. 79,380 reflections were measured for chR24 giving 18,142 unique reflections to 2.5 Å resolution (94% complete) with Rsym = 0.050. The protein crystallized in the monoclinic space group $C2$, with a = 146.8 Å, b = 56.0 Å, c = 80.0 Å and β = 119.2° The chR24-carbohydrate antigen was found to have crystallized in the $C2$ space group, with a single Fab per asymmetric unit and parameters for the unit cell of: a = 146.5 Å, b = 55.5 Å, c = 79.7 Å, and angle β = 119.2°, however no antigen density was apparent in the crystal structure.

3.3 R24-BEC2 binding studies

Protein A and size exclusion chromatography purification of a R24-BEC2 dimer complex were unsuccessful. SPR experiments performed at the NRC showed that the off-rate, that is the speed with which the antibodies separate after the initial binding, is high. Under size-exclusion chromatography such fast off-rates would suggest that the complex could not be purified because the antibodies did not form a stable complex under solution conditions. Under crystallization conditions the concentrations of both proteins are so high that the molecules spend most of the time in the complex form, and the the formation of the complex would be favoured.

3.4 R24 and chR24 binding studies

SPR experiments performed at the NRC showed that both R24 and chR24 bind GD3 bearing liposomes, but with greatly different affinities (Figures 16a and 16b). At concentrations of 2 μM, R24 gave a response of 1700 RU at the end of the injection while chR24 gave a response of only 35 RU. The apparent lack of saturation binding associated with R24 binding GD3 is the most interesting feature of the sensogram. This is

characteristic of homophilic binding and is similar to results previously reported for the binding of R24 IgG to human melanoma cell lines expressing GD3 (Chapman, 1990b). All concentrations of IgG showed complex binding kinetics, with distinctly biphasic behaviour evident at higher R24 concentrations (1 and 2 μM). and that in both cases an apparent lack of saturation of binding was observed and complex binding kinetics at all IgG concentrations. At high concentrations R24 and chR24 have biphasic behaviour. A "fast-binding" phase is observed to dominate in the first few seconds (70% of IgG bound), followed by a "slow-binding" phase which gradually increases the amount of bound antibody over a period of several minutes. The rapid initial association may reflect both GD3-antibody recognition and homophilic binding, with the slower association attributable solely to homophilic interactions. At lower concentrations R24 kinetics are simpler (Figure 16a inset), with biphasic behaviour not observed; however, even these data do not fit a simple bivalent analyte model. The data collected at lower IgG concentrations do fit well to a simple one-to-one interaction model, which gives an association rate constant of 1.3×10^{5} $M^{-1}s^{-1}$ and a dissociation rate constant of 2.3×10^{-3} s-1 (K_D = 18 nM). It was not possible to derive similar rate constants for chR24 because complex biphasic behaviour is observed at all concentrations (Figure 16b).

Scatchard analysis of equilibrium binding data obtained for the binding of murine R24 Fab to liposomes containing 10% GD3 is presented in Figure 17. The plot of bound *vs* bound/free R24 shows that homophilic binding was occurring, as a straight line with a

(a)

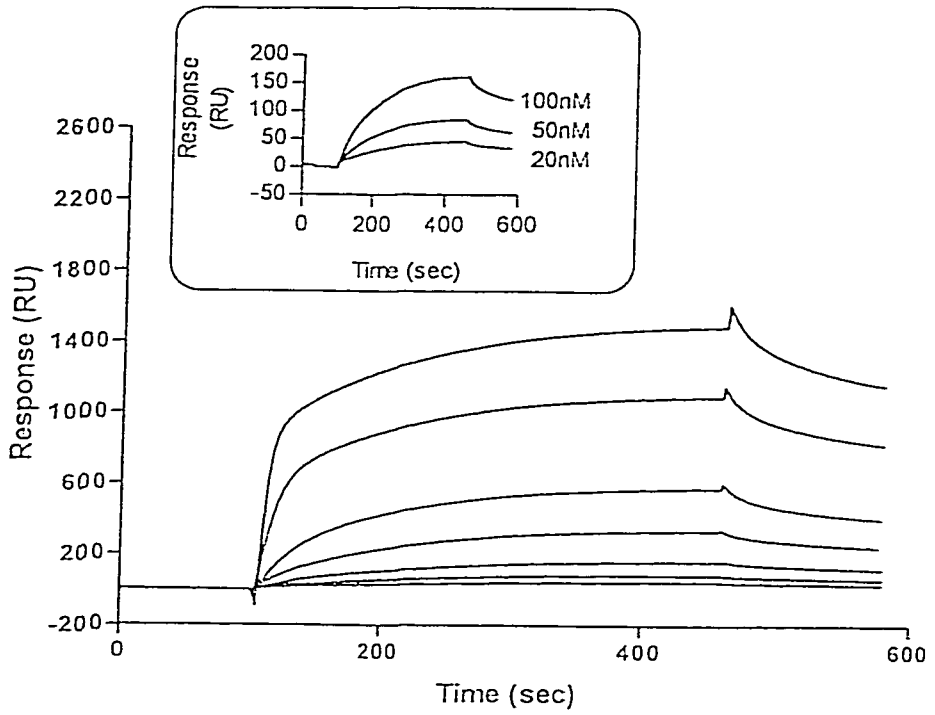

(b)

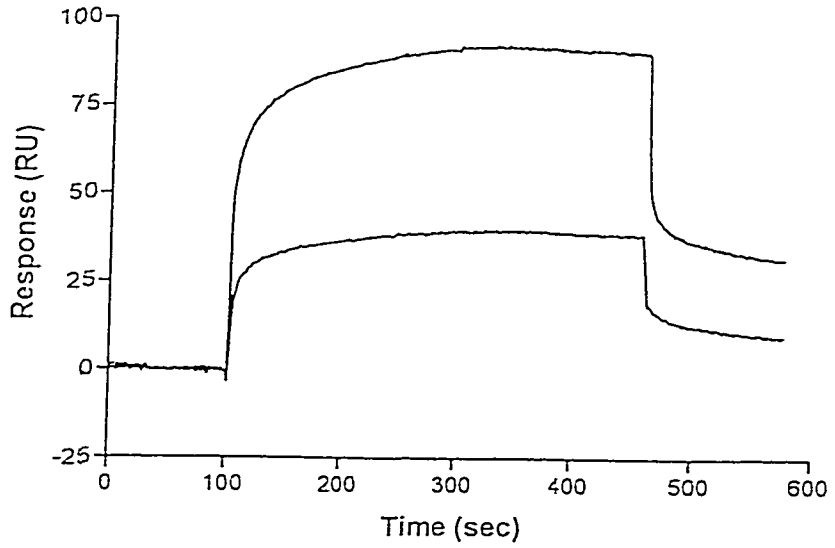

Figure 16: BIAcore sensogram results of R24 IgG binding to GD3 liposomes. (**a**) Murine R24 IgG at concentrations of 20, 50, 100, 200, 500, 1000 and 2000 nM. The inset shows an expanded y-axis for the lowest three concentrations. (**b**) Chimeric chR24 at concentrations of 2 and 5 μM.

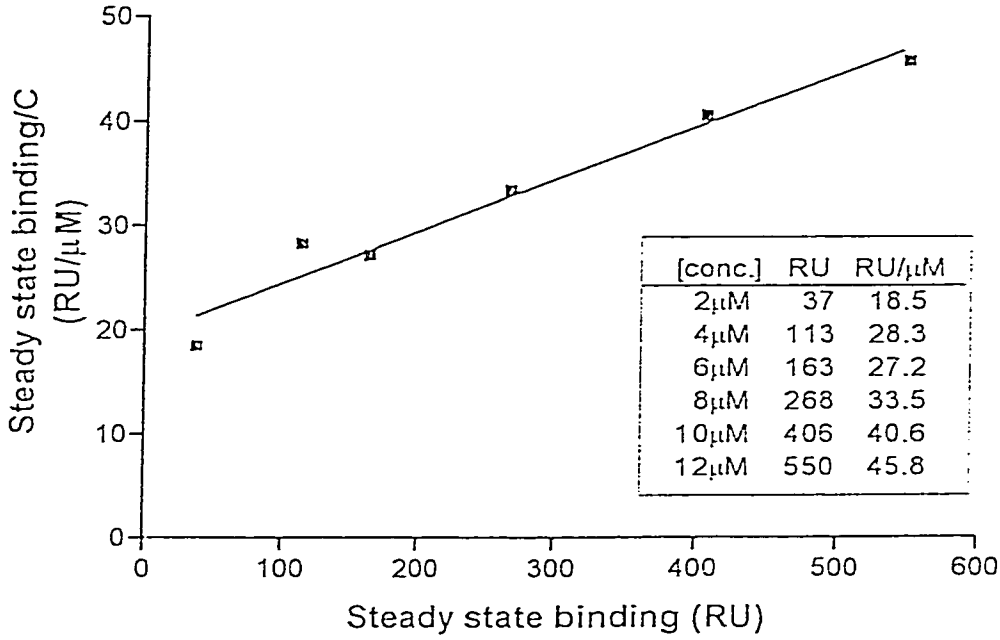

Figure 17: R24 Fab binding data. Scatchard plot of the equilibrium binding data for murine R24 Fab binding to liposomes containing 10% GD3. The equilibrium response, after control surface subtraction, at different Fab concentrations are given in the inset table.

positive slope indicates that proportion of available Fab that bound to liposomes is proportional to Fab concentration. The extent of the Fab dimerization resulting from homophilic binding would increase with concentration, and the resulting higher proportion of bivalent Fab would be manifested as an increased functional affinity. Equilibrium binding was achieved very rapidly at the Fab concentration used, and the dissociation of Fab from the liposomes was too rapid to allow the derivation of kinetic constants. These results also agree with reported experiments binding R24 IgG to human melanoma cell lines (Chapman, 1990b).

chR24 Fab affinity for GD3-bearing liposomes was significantly weaker than that of the murine Fab. A concentration of 80 μM gave an equilibrium response of 160 RU, for which R24 needed to be only at a concentration of 6 μM. A Scatchard plot of the equilibrium binding data obtained with chR24 Fab gave some indication of homophilic binding in that a line with no slope was obtained.

In contrast to GD3-bearing liposome studies, murine R24 IgG did not significantly bind to 12,500 RU (approximately 12.5 ng/mm^3) murine R24 IgG surfaces at concentrations as high as 1 μM, showing that in the absence of a GD3 bearing membrane there is no significant level of homophilic binding occurs. This contrasts with previous ELISA data which shows significant binding of 100 μg/mL R24 IgG to plates coated with 5 μg/mL R24 IgG per well (Chapman, 1990b). This may reflect that the IgG in the BIAcore® experiment is immobilized under conditions which more closely approximate a solution, while ELISA plates would present a more rigid two-dimensional environment more closely resembling a membrane surface.

4 DISCUSSION:

4.1 The R24 and chR24 Monoclonal Antibodies

R24 and chR24 antibodies are specific for the ganglioside GD3-NeuAc, which consists of 4 sugar residues (Neu5Ac-Neu5Ac-Gal-Glc) linked to a ceramide. R24 is a murine monoclonal IgG3 antibody, which in human trials has shown promise as a therapeutic agent for melanoma patients (Chapman *et al.*, 1990b; Ortaldo *et al.*, 1996; Minasian *et al.*, 1993; Vadhan-Raj *et al.*, 1988). ChR24 is a humanized form of R24 which retains the murine variable regions (V_H and V_L) conferring anti-GD3 activity, but with human constant regions (IgG1(κ)), in order to minimize patient immune response against the therapeutic antibody (LoBuglio *et al.*, 1989). The humanization was accomplished by ligating the genes coding for murine Fv onto the genes coding for the human constant domains (Yan *et al.*, 1996). Thus, R24 and chR24 Fabs share the same Fv region sequence but have different C_L and C_{H1} domains (Figure 18).

The structure determinations of R24 and chR24 were carried out in order to understand the nature of this important protein-carbohydrate interaction, and to understand the mechanism for homophilic binding displayed by R24, and to a lesser extent, chR24. This is the first report of the unliganded structures of both murine and chimeric antibody fragments. The two existing structural reports of chimeric Fabs deal either with an unliganded chimeric Fab (Brady *et al.*, 1992), or with a comparison of the liganded forms of murine and chimeric Fabs (Sheriff, et al., 1996), and neither of these systems display homophilic binding.

Figure 18: R24 and chR24 sequence alignment. Comparison of the R24 and chR24 sequences showing the differences in the constant domains between the murine and chimeric Fabs.

4.2 Comparison of R24 and chR24 crystal structures

4.2.1 X-ray crystal structure quality

The standard deviations of the distribution of bond lengths and bond angles from the theoretical values after the final refinement is 0.022 Å and 3.8° for R24, and 0.015 Å and 1.35° for chR24. Both structures have well-defined electron density over most of their respective polypeptide chains, even with the relative low resolution of the R24 data set. This includes the six CDRs of the single chR24 Fab and both R24 Fabs. The high quality of the low resolution R24 structure is particularly important as R24 was solved first, and this structure was then used for the solution of the chR24 structure.

4.2.2 R24 and chR24 antigen-binding surface

Both R24 and chR24 have a pronounced pocket or cleft in the antigen-binding surface located at the N-terminal side of the molecule (Figure 19). This pocket is large enough to accept the terminal GD3 antigen sialic acid residue (Figure 20). Antibody pockets have been organized by the profiles of their binding site structures into four groups: concave, moderately concave, ridged, and planar (MacCallum *et al.*, 1996). The R24 Fab antigen-binding pocket belongs to the concave group, and is entirely defined by the three heavy chain CDRs, which is unusual since both heavy and light chains are generally involved in antigen-specific interactions. The pocket on R24 is lined with four glycine residues, and predominantly polar amino acids: serine, threonine, histidine, and tyrosine. Specifically, the residues which contribute to the definition of the binding pocket are N31, G33 and H35 from H1; Y50, S52 and S53 from H2; and G99, G100, T101, G102, T103, R104, S105, L106, and Y107 from H3. The pocket has a pronounced

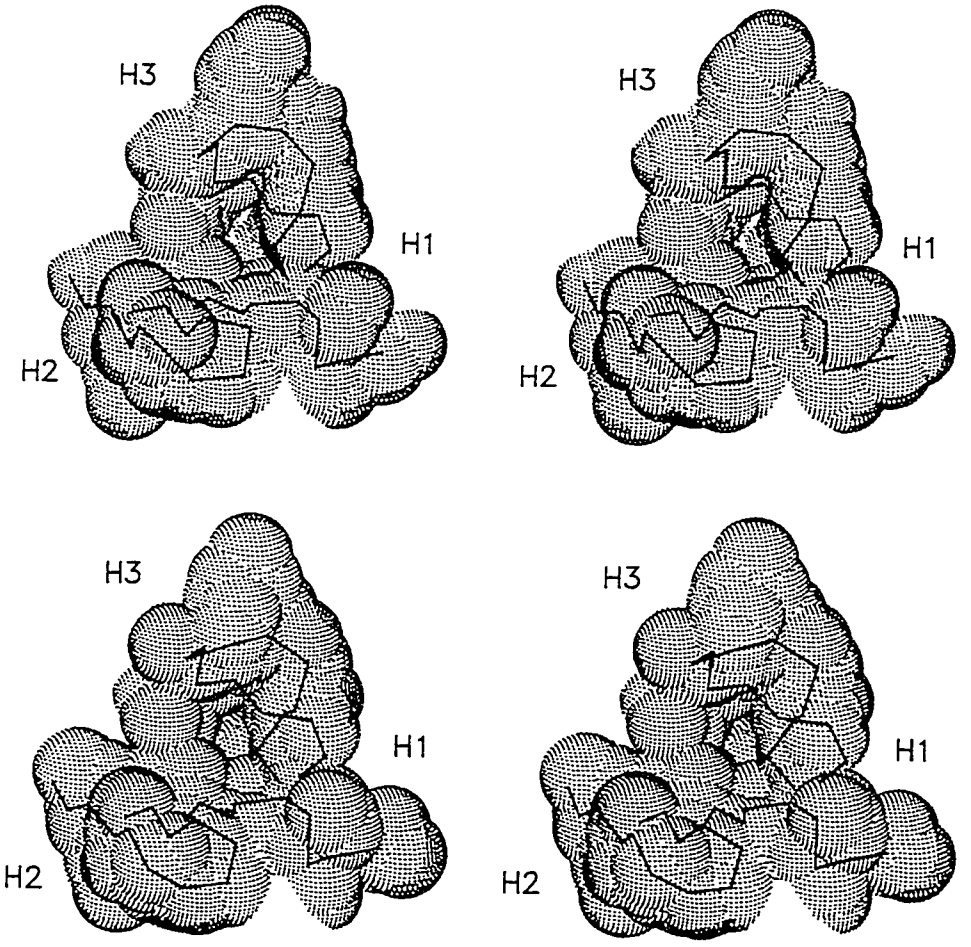

Figure 19: R24 and chR24 antigen binding sites. SETOR stereo representation of the R24 (top) and chR24 (bottom) N-terminal antigen binding pockets. The solvent-accessible surface area (red) and the heavy chain main chain α-carbon atoms involved in the formation of this pocket (black) are shown, specifying the positions of the heavy chain CDR positions.

Figure 20: SETOR stereo representation of the Fab binding pocket with GD3 terminal Neu5Ac residues. The cut-away view shows the position of the terminal Neu5Ac N-acetyl moiety which can penetrate to the bottom of the pocket surface. GD3 model is shown in thick lines, chR24 H2 loop in thin, antibody surface is in gray.

mouth which includes residue S53. Mutations of this residue have been correlated previously with a loss of GD3 antigen-binding and/or of homophilic binding (Yan *et al.*, 1996).

4.2.3 Comparison of atomic position of R24 and chR24

The Fv regions of R24 and chR24 have 100% sequence homology, and it is not surprising that only small variations in the main chain and residue positions are observed (Figure 21). A least-squares superpositions of the α-carbon atoms of the Fvs of chR24 onto either Fv from R24 gives an rms deviation of less than 1.0 Å (less than 0.57 Å for residues lining the GD3-binding pocket), and shows that the humanization process has no significant effect on the conformation of the Fv. Most of the observed differences between the murine and chimeric structures are probably due to coordinate errors for the lower-resolution R24 structure, and there is little real difference between the two structures.

R24 crystallized with elbow angles (i.e. the angles subtended by the two pseudo-twofold axes of the Fv and first constant region) of 166.7° and 167.3° for the two Fabs in the asymmetric unit, respectively, while chR24 is similar with an elbow angle of 171.5°. Thus, the variable and constant domains have virtually the same orientation and place in both the chimeric and native form of R24. Since the elbow angle has been implicated in allosteric induction of the antigen binding response from the variable to the first constant domain (Guddat *et al.*, 1994), minimization of changes to this region may be important when creating a functional chimeric Fab.

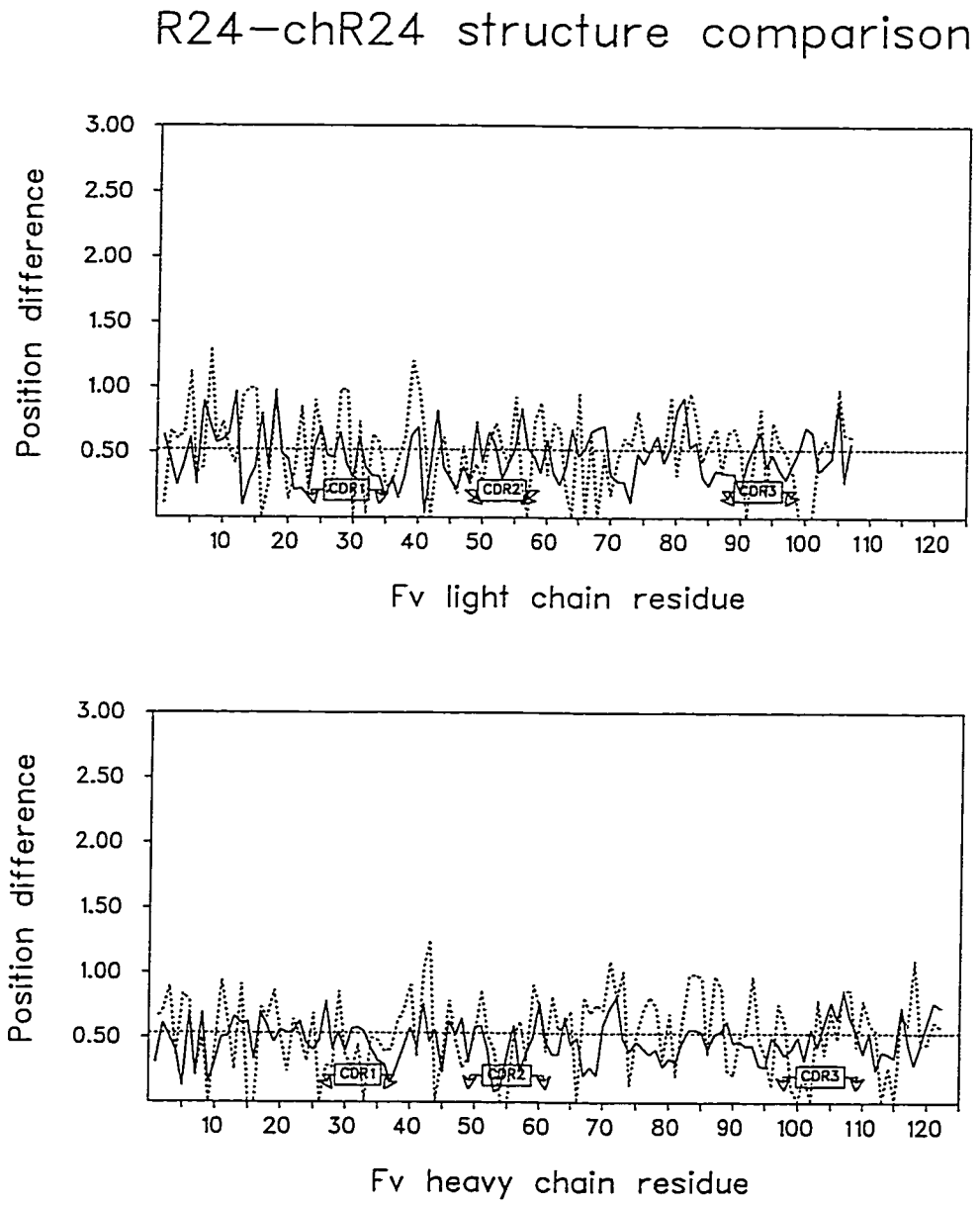

Figure 21: Comparison of light and heavy chain atom positions between R24 and chR24. The difference in position between the main chain (solid) and side chain (dotted) positions of the murine and chimeric Fab. The average difference in side chain position is shown as a horizontal dashed line.

4.2.3 Location of ID_{GD3}

Since experiments to soak the GD3 ligand into the chR24 crystals before data collection did not yield interpretable electron density, a model of GD3 binding to the R24 binding site was developed. The pocket formed by R24 CDRs measures approximately 8.5 x 12 x 8 $Å^3$, providing accommodation for the terminal sialic acid residue of GD3. A model of the terminal sialic acid residue was fit into the observed pocket so as to achieve maximum complementarity between the antigen and the surface of the pocket. Figure 22 shows the fit of antigen model to antibody structure, where the modelled GD3 residues show a good fit based on size, structure, and potential hydrogen bonds. The terminal N-acetyl group on C5 of the terminal Neu5Ac residue is long enough to interact with the residues lining the bottom of the pocket. Hydrogen bonds can be formed between the antigen model and residues S53, Y50, T103, R104, S105 and Y107. The hydrogen bonding is not limited to the terminal Neu5Ac residue as the second modelled Neu5Ac residue can form at least two hydrogen bonds with R24, as can the glucose.

4.2.4 Sequence analysis of BEC2

BEC2 is a monoclonal antibody raised in mice in response to immunization with R24, and is a true type-β anti-idiotypic antibody mimic of the GD3 antigen (Chapman & Houghton, 1991). Trials of BEC2 as an immunizing agent showed induction of anti-GD3 activity in rabbits (Chapman & Houghton, 1991) and humans (McCaffrey *et al.*, 1996). BEC2 Fab presented problems during purification and crystallization, primarily due to the presence of a secondary light chain produced in the BEC2 hybridoma, and no crystals of BEC2 cound be generated. A model of BEC2 was constructed in order to determine the

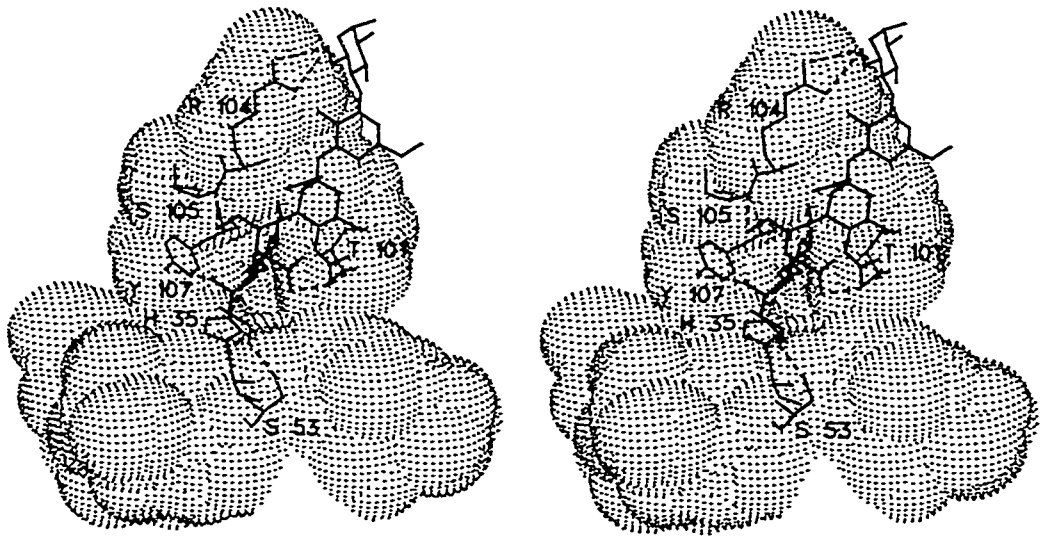

Figure 22: R24-GD3 interaction model (stereo). SETOR representation of the GD3 model bound into the R24 specificity pocket showing possible hydrogen bond interactions with main chain and side chain atoms of R24. THe GD3 extends along the surface of the antibody towards the membrane surface. GD3 is shown in black, R24 surface in light gray, R24 residues in dark gray, and hydrogen bonds are represented by dashed lines.

location of possible GD3-mimicking sites (presumed to be one of the CDR loops, given the size of the GD3-binding pocket on R24).

The known sequence of BEC2 was modelled onto the previously solved Fab structure of YSt9-1, an anti-oligosaccharide antibody (Rose *et al.*, 1994; Evans *et al.*, 1994). The modelled L1 CDR was the only CDR that could form an extended loop structure capable of sampling the entire surface of the anti-GD3 pocket (Figure 23). The extended L1 sequence is a 5-residue peptide segment with the sequence LDSDG. Comparison of this sequence with peptides known to be immunologically active showed similarity with the human IgM pentapeptide known as Hamburger peptide (DSDPR) (Hamburger, 1975; Hahn, 1986), leading to crystallization trials with both the Hamburger pentapeptide and the BEC2 pentapeptide. These crystallization trials are still underway, but were not complete at the time of thesis writing, and so modelling of the L1 loop into the GD3-specific pocket on R24 was undertaken.

The model of the BEC2 L1 loop could be satisfactorily fit to the antigen binding pocket, with two charged and one polar residues (D31, S32, D33) capable of forming a number of hydrogen bonds with R24 residues H35, T101, and S105 (Figure 24). The side chain of D31 extending to the bottom of the GD3 antigen-binding pocket is reminiscent of the interaction of the terminal N-acetyl group on GD3.

4.2.5 Comparison of modelled GD3 and BEC2 antigens.

One of the most intriguing features of the BEC2 L1 loop is the presence of two closely-spaced negatively charged residues, which immediately brought to mind the carboxylic acid groups on the two Neu5Ac residues of GD3. However, although the

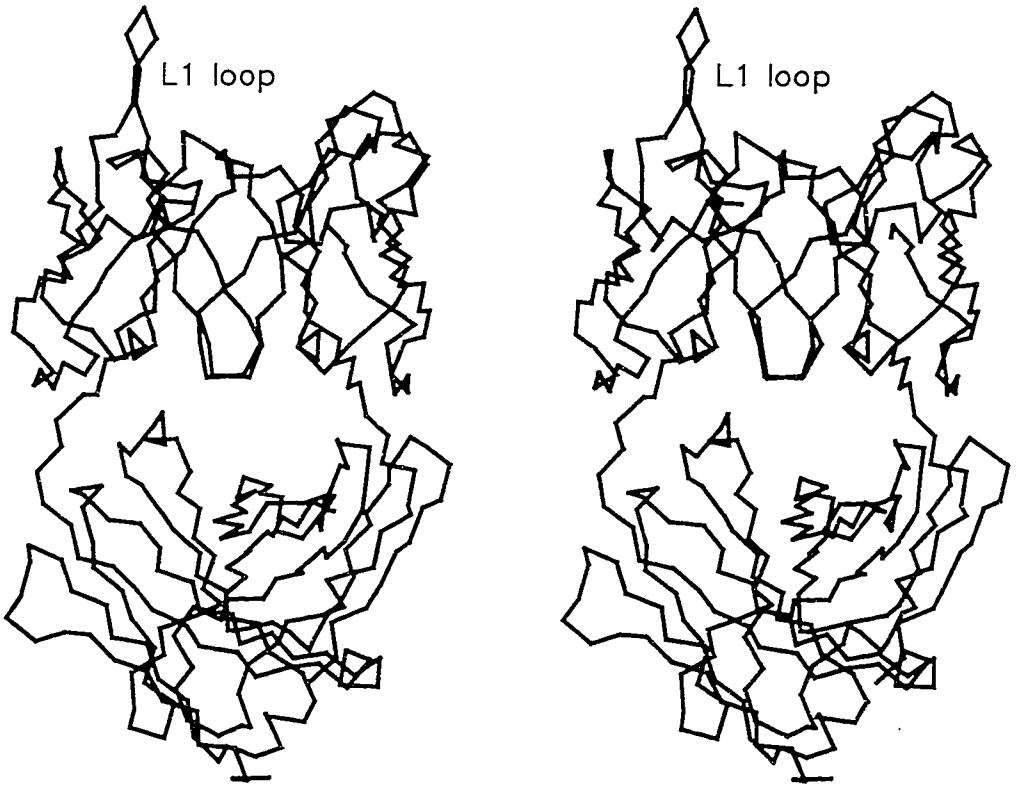

Figure 23: BEC2 Fab model α-carbon representation (stereo). SETOR representation of the BEC2 model showing the extended loop conformation possible for L1 CDR.

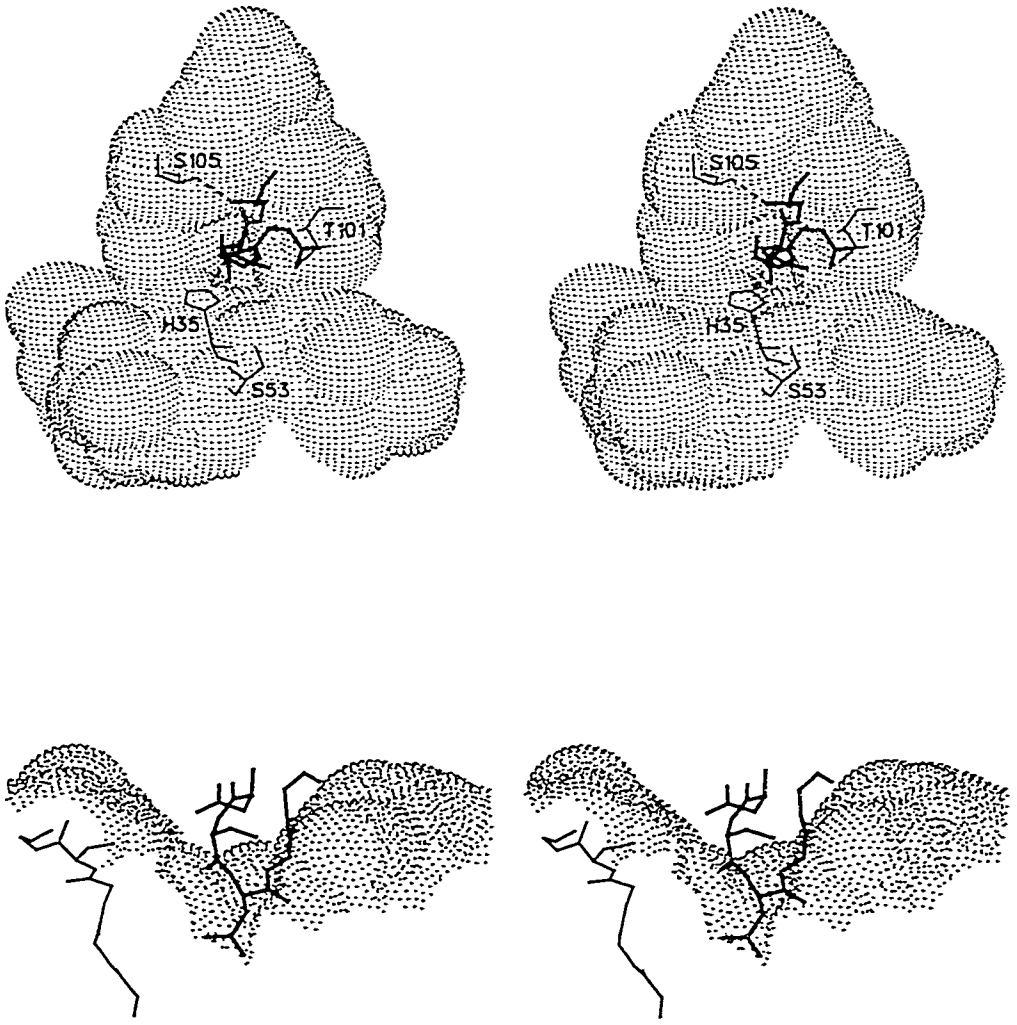

Figure 24: BEC2 - R24 binding model (stereo). SETOR representation of possible interaction between BEC2 L1 CDR and the GD3-specificity pocket of R24. (**a**) The top view showing possible hydrogen bonds between BEC2 (thick) and R24 (thin); the R24 surface is shown in light gray. (**b**) The cut - away side view shows that BEC2 (thick) can penetrate to the bottom of the specificity pocket surface (light gray).

modelled Neu5Ac residues and BEC2 antigenic loop are capable of forming similar hydrogen bond interactions with the GD3-binding pocket (Figure 25), with both showing a high degree of complementarity, no model could be found that yielded a similar distribution of charge. There are no residues with explicit positive charges lining the surface of binding pocket on R24 which might complement the charges on the antigen. His-35 has the potential to contain a positive charge, but is positioned at the bottom of the pocket, and would not be in a position to form a salt bridge with GD3 residues.

The modelling of BEC2 was abandoned at this point in order to concentrate on the mechanism of homophilic binding.

4.2.6 GD3 Binding and Homophilic Binding Have Distinct Epitopes

Several R24 mutants were assayed at Sloan-Kettering for both GD3 binding and homophilic binding (Yan *et al.*, 1996). These R24 mutants include S53T, S53R, S53P, S53D and S53Y, and D62Q, and D62H. Two double mutants were also investigated S53R-D62E and S53P-D62Q. ELISA assay data for homophilic and GD3 binding are presented in Table 4.1. The most interesting mutation proved to be the S53T substitution, which maintained GD3 binding, albeit at a lower avidity, while disrupting homophilic binding activity (Yan *et al.*, 1996). This indicated that the sites responsible for binding GD3 (ID_{GD3}) and for homophilic binding (ID_{HOM}) were related to the H2 loop, but were distinct (Yan *et al.*, 1996).

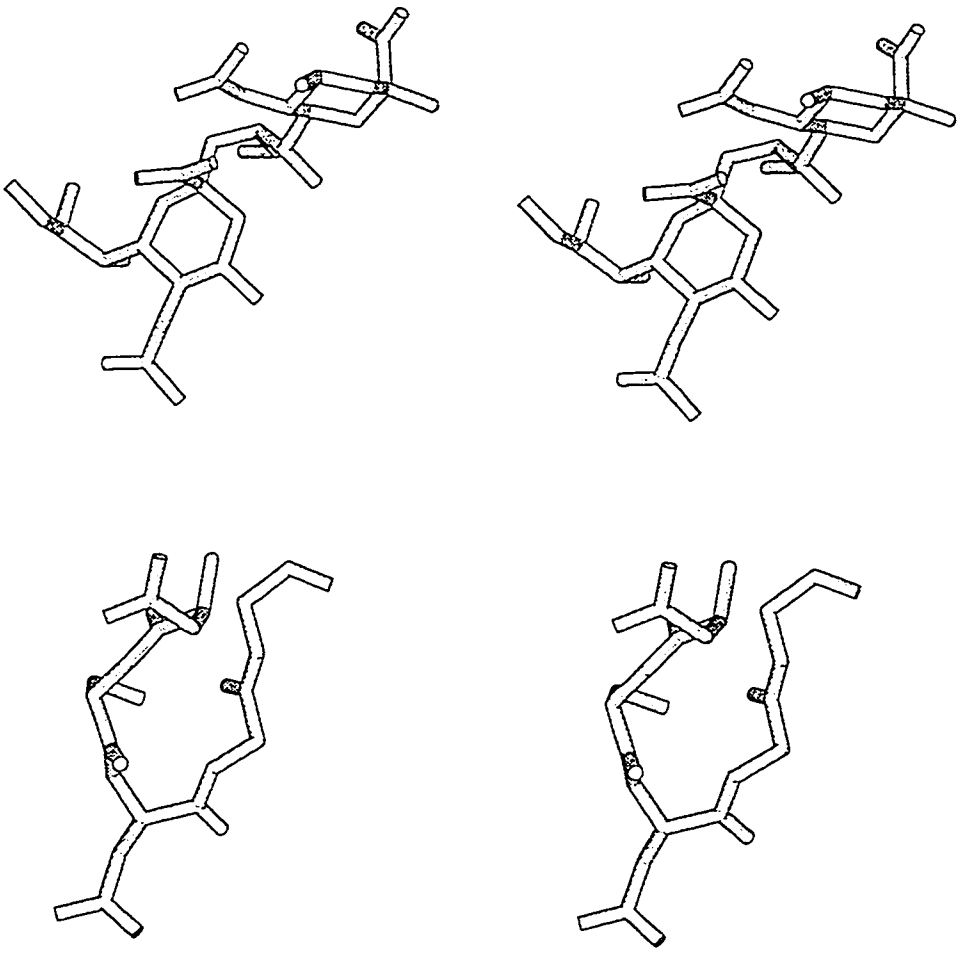

Figure 25: Comparison of the models of GD3 and BEC2. SETOR representation of the antigen models showing the orientation both have in the antigen-antibody interaction models. GD3 is shown on top, BEC2 is shown on bottom.

Table 4.1 Homophilic Binding of chR24 Mutants

chR24 variant	homophilic binding	binds GD3
native	+	+
S53T	-	+
S53R	-	-
S53P	-	-
S53D	-	-
S53Y	-	-
D62Q	+	+
D62H	+	+
S53R, D62E	-	-
S53P, D62Q	-	-

Structural data for the mutants were generated by modelling the mutations onto the solved R24 structure. These models were compared to one another and to the model of the native Fab bound to GD3. The S53T mutation involves the smallest change in the side chain of any of the mutants, where an H is exchanged for a CH_3 group while maintaining the hydroxyl group. This mutation would produce a bulge in the mouth of the GD3-binding pocket, and would partially occlude the binding site. However, the modelled increase in surface area occurs in such a way as not to interfere with the GD3 interaction with the pocket (Figure 26). Other mutations clearly produce a large obstacle to antigen entering the binding pocket, and it is easy to understand why these changes eliminate GD3 binding. For example, the S53R mutation is shown in Figure 27.

4.2.7 Identification of ID_{HOM}

The point mutation studies in Yan *et al.*, 1996 clearly show that homophilic binding is associated with the H2 loop. Although SPR studies showed that this interaction is relatively weak compared to other protein-protein interactions, it is a

Figure 26: chR24 S53T mutant. SETOR stereo representation of the change in surface accompanying the S53T mutation shown in a cut away view of the pocket. The GD3 model (green) can bind into the pocket of native R24 (red). The altered S53T mutant surface (blue) changes the lip of the pocket but does not interfere with the GD3 binding model.

Figure 27: chR24 S53R mutant. SETOR stereo representation of the change in surface accompanying the S53R mutation shown in a cut away view of the pocket. The GD3 model (green) can bind into the pocket of native R24 (red). The altered S53R mutant surface (blue) occludes the binding pocket, preventing GD3 binding.

specific interaction, and would be expected to dominate the packing interactions found in the lattice of crystals of the unliganded Fab of R24 and chR24. An examination of the crystal structures of both the murine and chimeric Fabs shows that they are packed in a head-to-head orientation with neighbouring molecules in the crystal lattice. An examination of the crystal structures available in the Protein Data Bank (Bernstein *et al.*, 1977) shows that such head-to-head interactions are uncommon, with most Fab crystallizing in a head-to-tail arrangement. This unusual packing mode is derived from an intermolecular antiparallel β-sheet interaction between a 5-residue portion of the H2 framework β-sheets of both Fabs, extending from S56 to Y60 (Figure 28).

This intermolecular interaction is found in the packing of the crystals of the Fabs from both R24 and chR24. R24 crystallizes in space group $P2_1$ with two Fabs per asymmetric unit (dubbed Fab1 and Fab2). This means that there are two Fab molecules in the unit cell that are not related by any crystal symmetry. The space group $P2_1$ contains one unique symmetry element (a two-fold screw axis), which generates two additional molecules in the unit cell (dubbed Fab1' and Fab2'). Thus, there are four molecules in the unit cell of the R24 crystal structure. Interestingly, both independent Fabs in the crystal structure display similar antiparallel β-sheet interactions, with Fab1 interacting with Fab2' (i.e. a symmetry-related Fab2), and Fab2 interacting with Fab1', Figure 29.

Fabs of chR24 crystallized in a different space group, *C*2, which means that the packing arrangement of the molecules would be expected to be different. Nevertheless, the same β-sheet interaction is also present in this structure, showing that both R24 and chR24 Fabs are crystallizing as dimers. The Fabs of chR24 crystallize with one molecule

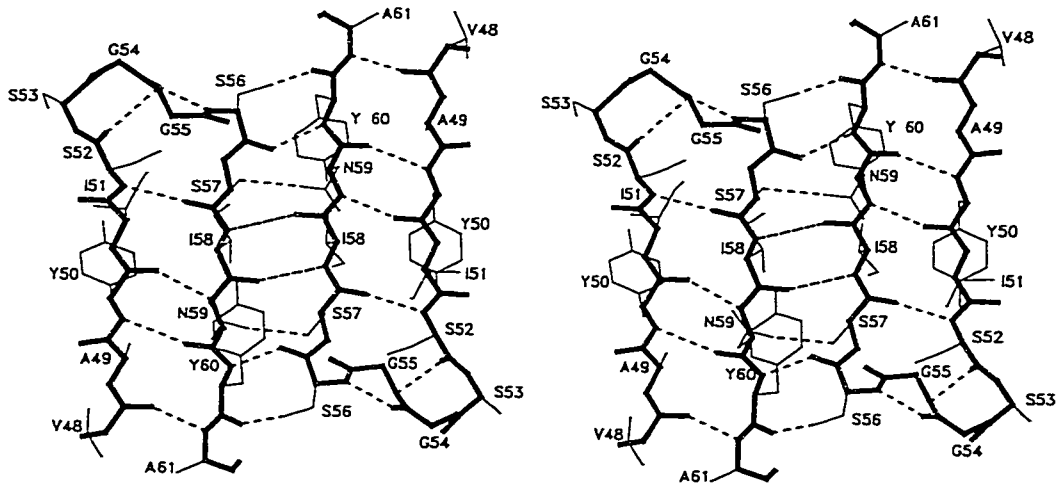

Figure 28: chR24 CDR H2 ID_{HOM} dimerization. SETOR stereo representation of the are of dimerization between molecules of chR24 in the crystal lattice, with the positions of the main chain (thick) and side chain (thin) atoms as well as observed hydrogen bonds (dashed). Amino acids of each H2 loop are labelled with their residue number and corresponding 1-letter codes. The interactions are simillar to those observed in the R24 dimer.

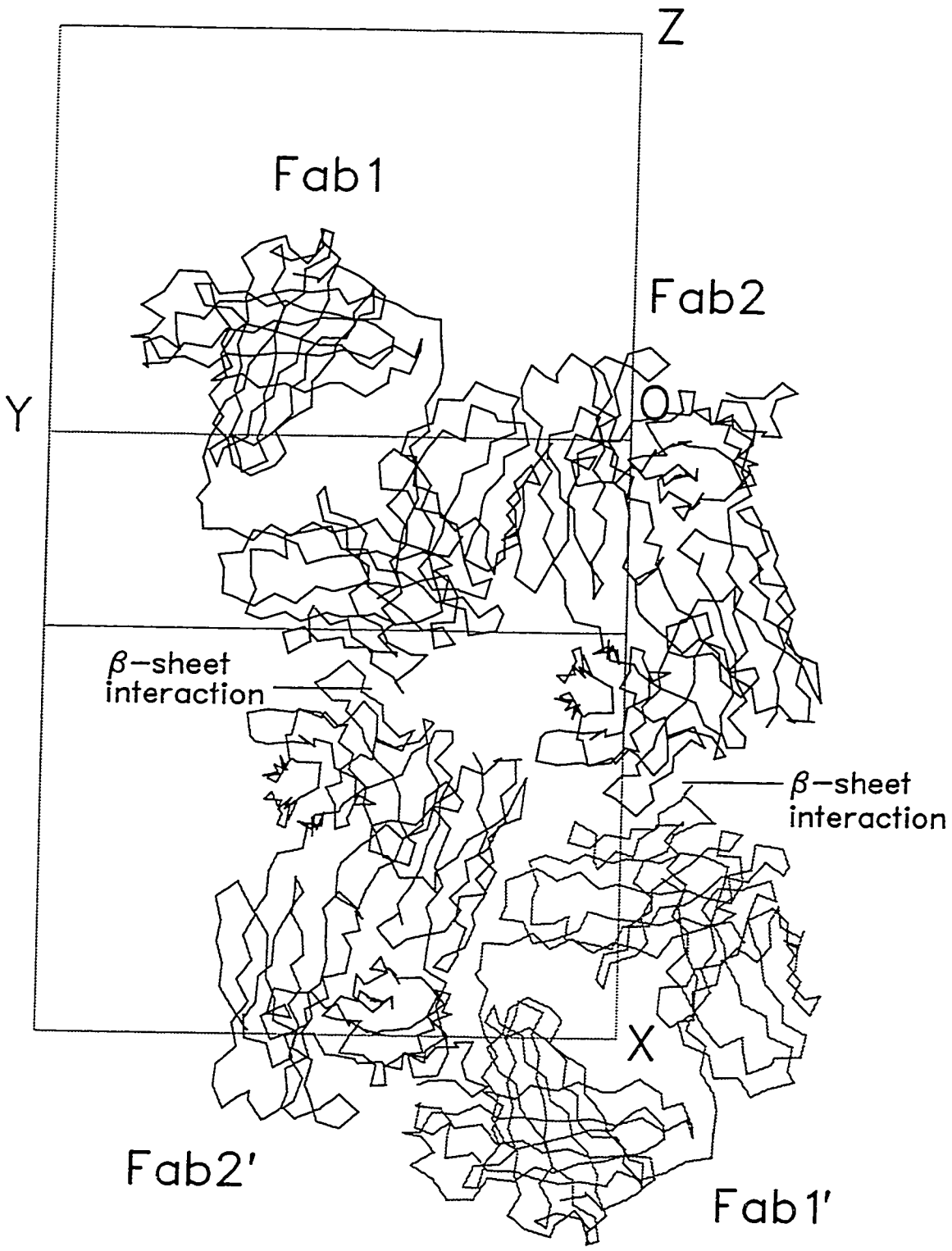

Figure 29: R24 Fab interactions and unit cell. SETOR representation showing the main chain interaction between Fab in the R24 crystal structure. Shown is the head tohead interaction between Fab1 and Fab2' and Fab2 and Fab1'. The unit cell (dashed) with axis labels is shown.

per asymmetric unit, and the β-sheet dimerization interaction occurs between symmetrically related Fab molecules (Fab and Fab') (Figure 30). The intermolecular contacts made by R24 and chR24 differ outside the β-sheet dimerization region. R24 shows various heavy and light chain interactions while chR24 displays predominantly interactions between V_L and C_{H1} domains of neighbouring Fabs.)

The fact that the same interaction is observed in three different pairs of Fab molecules in two different crystal structures, combined with the point mutation studies that localize homophilic binding to the H2 loop, indicates that this antiparallel β-sheet interaction is the site for ID_{HOM}. Table 4.2 contains a list of the hydrogen bonds observed at the dimer interface.

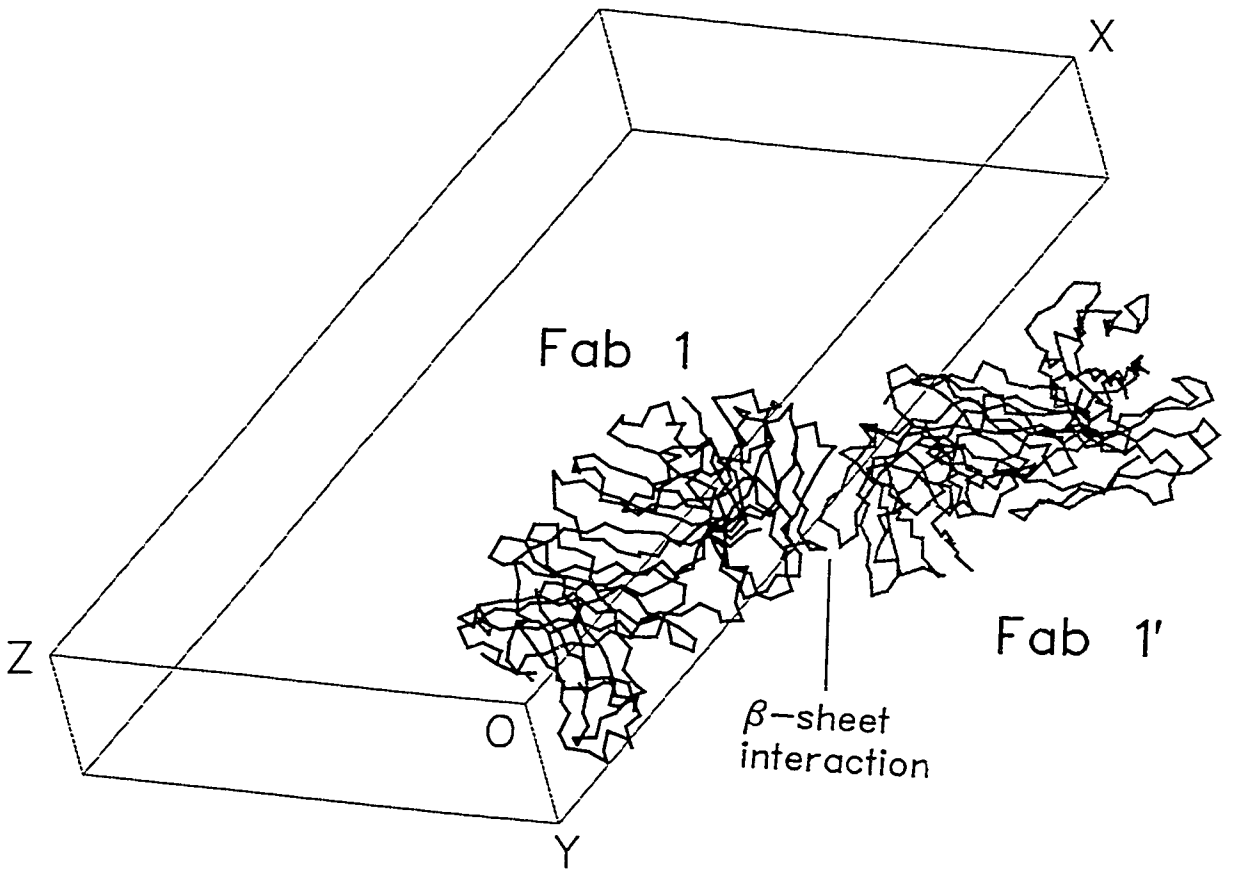

Figure 30: chR24 Fab interactions and unit cell. SETOR representation of main chain interaction between symmetry related asymmetric units of chR24. Shown is the head to head interaction between Fab and Fab'.

Table 4.2 Intermolecular interactions found along the H2-loop interface of R24 and chR24 in the crystal lattice

main chain-main chain hydrogen bonds						hydrogen bond distance (Å)	
						R24	chR24
Ser	H 56 O	...	NH	Tyr	H 60	2.89	3.08
Ile	H 58 N-H	...	O	Ile	H 58	3.37	3.03
Ile	H 58 O	...	NH	Ile	H 58	3.87	3.03
Tyr	H 60 O	...	NH	Ser	H 60	2.84	3.08
hydrogen bonds involving side chain atoms							
Ser	H 56 OH	...	O	Tyr	H 60	2.93	2.61
Ser	H 56 N	...	OD1	Asp	H 62	3.46	n.o.
Ser	H 57 OH.	...	H-ND	Asn	H 59	3.01	2.78
Asn	H 59 ND-H	...	HO	Ser	H 57	2.78	2.78
Tyr	H 60 O	...	HO	Ser	H 56	n.o.	2.61
potential hydrophobic interactions							
Ile	H 58	...		Ile	H 58		4.4

n.o. = not observed.

In addition to the classic main chain-main chain hydrogens bonds which define a β-sheet, there are several hydrogen bonds involving side chain atoms which serve to stabilize the dimer. There is also an observed hydrogen bond between the side chain of D62 and the main chain of S56; however, this interaction does not play a critical role in homophilic binding as it can be mutated without apparent effect (see Table 4.1, above).

There is one potential hydrophobic intermolecular interaction between I58 and I58'. At 4.4 Å this contact is too long to be significant in the crystal structure, but it may

come into play in solution binding. The angle between the pseudo two fold axes of the two Fvs in the dimers are 167° in R24 and 155° in chR24, showing that the dimer has some flexibility. Modelling the freedom of rotation about the axis of the β-sheet shows that the dimer can flex through approximately 20° without generating significant steric interactions.

Edmundson and Borrebaeck (1998) have recently proposed that interactions observed between constant regions in the crystal structures of several Fabs do not depend on side chain identities, however, the side chain interactions observed for R24 and chR24 do participate in the stabilization of the β-sheet dimers.

4.2.8 β-sheet and canonical CDR H2 structures

An examination carried out using the SETOR program package of the 74 Fab, Fv, and IgG structures in the Protein Data Bank (or PDB, Bernstein *et al.*, 1977) solved to 3.0 Å resolution or better showed that the sort of head-to-head β-sheet interaction exhibited by R24 is rare. Only one other structure (HIL, Saul & Poljak, 1992, accession 8FAB) displays β-sheet dimerization through the variable domains of the antibody, and that also occurs through the H2 loop.

The topography of CDR structures has been divided into canonical conformations (Chothia *et al.*, 1987; Chothia *et al.*, 1989), of which four conformations have been identified for H2 (Figure 31). All of the conformations of H2 loop reported in the PDB are observed to fall into one of the four categories. To a great extent, the conformation of the H2 loop has been found to be dependent simply on the length of the loop. Given the

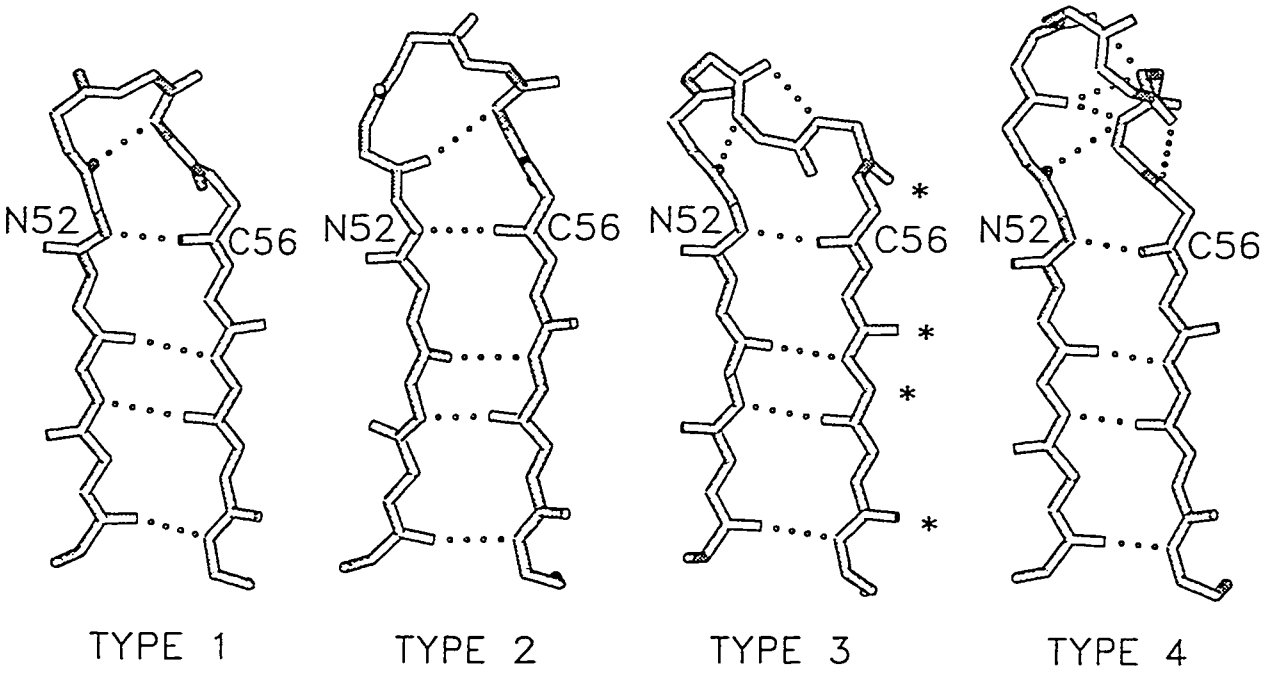

Figure 31: Complementarity determining region H2 canonical structures. SETOR representation of the four types of canonical structures possible for the H2 CDR (Chothia *et al.*, 1989). The difference in the loop structures stem from the number of residues in the hypervariable loops (3 in Type 1, 4 in Type 2 and 3, 6 in Type 4) and from the loop conformations (Type 2 and Type 3). Only Type 3 loops have all main chain hydrogen bonding groups oriented to form -sheet dimerization (shown by asterisks). Both R24 and chR24 structures are characteristic of Type 3 H2 loops.

length of H2 as defined using Kabat numbering in Chothia *et al.*, 1987, canonical forms 1, 2, 3, and 4 are formed by loops of length 3, 4, 4, and 6 residues, respectively. An examination of each loop type was carried out to determine which can form the intermolecular β-sheet interaction.

R24, which has 4 residues separating the framework residues 52 and 56 (Kabat numbering), belongs to Type 3 canonical structures. Comparison of the Type 3 structure to canonical forms 1, 2 and 4 shows that only Type 3 loops have main chain atoms positioned for possible β-sheet dimerizations. Type 1, Type 2 and Type 4 loop models are capable of forming a single pair of hydrogen bonds through the main chain atoms. Modelling of the four loop types shows that Type 4 loops may be capable of forming a set of hydrogen bonds at a different position that Type 3 loops; however, no structures displaying such interactions have been reported.

Of the antibody fragment structures reported in the PDB, only Fab HIL (a human myeloma protein) showed a head-to-head interaction through the V_H domains. HIL also contains a Type 3 H2 CDR loop, and forms a β-sheet similar to that found in R24, with Fab1 interacting through a pseudo 2-fold axis with Fab2'. Although the interaction is similar to that seen in R24, Table 4.3 shows that the residue identities are different, but that side chains are again significantly involved in the interaction.

Table 4.3 Intermolecular interactions found along the H2-loop interface of HIL

main chain-main chain hydrogen bonds						hydrogen bond distance
Ser	H 56 O	...	NH	Tyr	H 60	2.89
Thr	H 58 N-H	...	O	Thr	H 58	3.13
Thr	H 58 O	...	NH	Thr	H 58	3.25
Tyr	H 60 O	...	NH	Ser	H 60	2.88
hydrogen bonds involving side chain atoms						
Asn	H 54 O	...	H-NZ	Lys	H 65	3.17
Arg	H 57 DN-H	...	O	Tyr	H 59	3.03
Lys	H 65 ZN-H	...	O	Asn	H 54	2.97

Unlike R24, there are no hydrophobic residues which have the potential to interact across the dimer interface.

It is of interest to examine the possible factors which contribute to β-sheet dimerization across the H2 loop given the limited number of structures which display this phenomenon. For example, the presence of the Type 3 canonical form for H2 is not a limiting factor in the display of homophilic binding, as there are 23 structures in the PDB which have H2 loops which display Type 3 canonical forms. As well, the homophilic binding interaction is not a function of the space group in which the antibody fragments crystallized. Only one (R24) of 10 structures in space group $P2_1$, one (chR24) of 7 structures in space group $C2$, and one (HIL) of 26 structures in space group $P2_12_12_1$ crystal structures in the PDB database showed β-sheet dimerization through their variable domains.

domains.

Primary structure is, of course, the defining aspect of any protein, but the primary structure of the H2 loop alone does not appear to be a critical factor in homophilic binding. The R24 and HIL antibodies do not share any sequence homology in their H2 loop, yet both display β-sheet dimerization. The four Fabs of known structure which share the closest sequence similarity with R24 CDR H2 are not observed to crystallize in the head-to-head manner of R24 and HIL. However, in these cases an examination of the molecular structures of these Fabs shows that steric interference between side chains and main chains and between main chains of the homophilic binding region and other parts of the protein would prevent close approach of the H2 loops.

In addition to R24 there are four murine monoclonal antibodies from Sloan-Kettering which are directed against GD3 binding family and which also display ID_{HOM}. These are coded C5, 11A, MB3.6, and K9 (Table 4.4). Structure determination of these proteins has not been undertaken, and so the sequence of each protein was modelled onto the solved R24 structure using the SETOR program. Of the GD3 binding antibodies which express ID_{HOM}, including R24 and chR24, only one does not have a sequence which could form a Type 3 H2 loop (Chapman et al., 1990b; Yan et al., 1996). The modelling of ID_{HOM} of the three Fabs loop sequences consistent with canonical form 3 (C5, 11A, MB3.6) showed that homophilic binding could occur across the H2 interface with no side chain steric hindrance. Antibody K9 has two extra residues in the H2 CDR, which almost certainly exists in a Type 4 H2 canonical form. K9 shows R24 binding only at relatively high concentrations, and must therefore form a weaker interaction with

R24 than the other antibodies.

Table 4.4 CDR H2 sequence comparison of ID_{HOM} expressing anti-GD3 mAb

	50 53	56 58 60 62	ID_{GD3}/ID_{HOM}
R24	Y I S S	G G S S I N Y A D T V K	+/+
C5	Y I S S	G G S T I Y Y A D T V K	+/+
11A	T I S S	G G S Y T Y Y P D S V K	+/+
MB3.6	T I S S	G G S H T Y Y P D S V K	+/+
K9	E I R S K A	N Y H A T Y Y A E S V K	+/+
HIL	V I W Y	N G S R T Y Y G D S V K	?/+

The effect that mutation of residue S53 has on the binding of GD3 is clearly explained by examination of the crystal structure (see 4.2.6, above). However, it is less obvious why these mutations disrupt homophilic binding, while single point mutations for residue D62, which is physically closer to the site of β-sheet dimerization, do not disrupt homophilic binding. It is possible that the mutation of S53 causes small changes in the conformation of the H2 loop, perhaps to change it to a canonical type 2. A second possibility is that the conformation of the H2 loops is not affected, but that mutation of S53 causes a reorientation of side chains near the dimerization interface that disrupts binding. In any case, although very different residue identities can still lead to β-sheet dimerization in R24 and HIL, it is clear that the assertion that primary structure is not critical in the formation of antibody-antibody interactions (Edmundson and Borrebaeck, 1998) is not strictly true.

4.3 R24 Recognition of Transformed Cells

4.3.1 GD3 and homophilic binding stabilization on the cell surface

The fact that the antigen-binding and homophilic binding sites are distinct has a profound impact on the ability of R24 to bind GD3 in a membrane environment like the surface of a transformed cell, because it means that each molecule of R24 can simultaneously bind to antigen and to another molecule of R24. The dimer found in the crystal structure of the Fabs of R24 and chR24 immediately suggests a model of antigen binding on cell surfaces.

The optimum orientation of the Fab dimer to allow simultaneous homophilic and GD3-binding would maintain the H2 loop "up" away from the membrane surface. This would leave a clear path for the membrane-bound GD3 antigen to reach the antigen-binding pocket (Figure 32). This model requires that light chains of the Fab be in proximity to the cell surface. Previous studies have shown that although the R24 heavy chain is responsible for the actual GD3 antigen-binding and homophilic binding, the idientity of the light chain can enhance binding. For example, the substitution of a single R24 IgG light chain by an MOPC21 light chain causes a 40 fold decrease in GD3 avidity (Chapman *et al.*, 1990a). R24 contains a tryptophan residue at position 65 in the light chain which is exposed to the solvent (Figure 33). In the model, W65 would be in a position to intercalate into the phospholipid surface, which might aid in the stabilization of the GD3-bound antibody on the cell surface. This could be tested by site-directed mutagenesis, and the generation of a recombinant mutant protein.

4.3.2 Surface Plasmon Resonance

Both the chR24 IgG and Fab shows reduced GD3 binding compared to the corresponding R24 molecules, suggesting that the changes in binding between the two

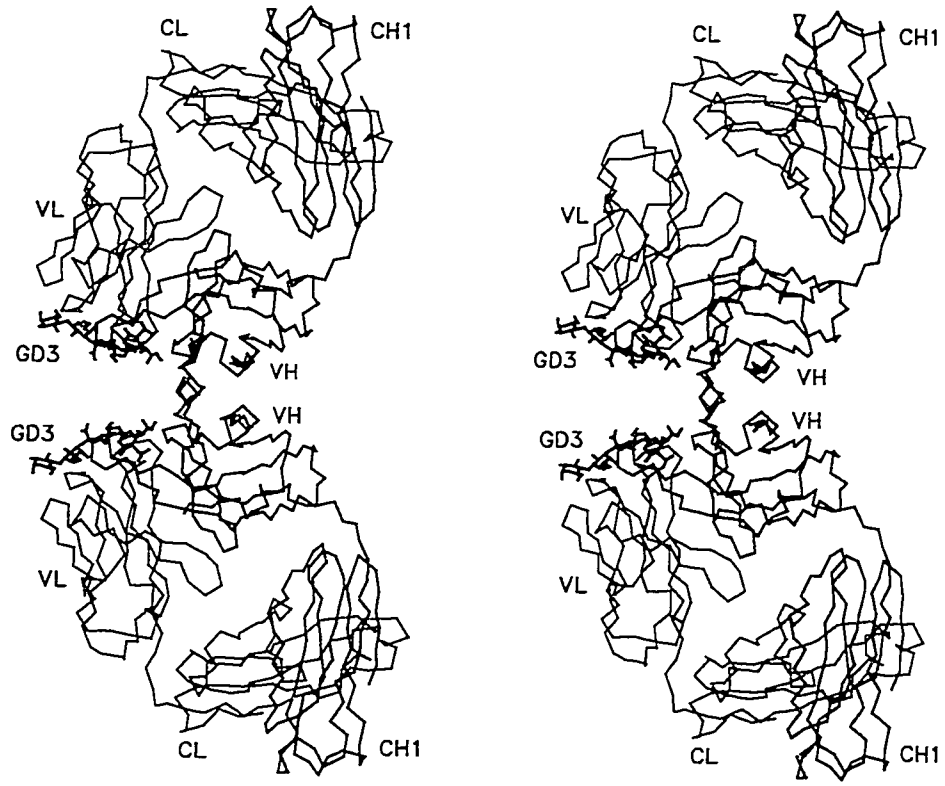

Figure 32: chR24 Fab dimer. SETOR stereo representation of the α-carbonbackbone of the chR24 dimer showing the relative positions of the light (gray) and heavy chains (black). The GD3 model (red) is positioned such that the terminal Neu5Ac reside lies in the pocket observed on the surface of R24, with the four sugar residues of the antigen extending towards the "side" of the antibody (left) where the ceramide moiety would lie buried in the cell membrane.

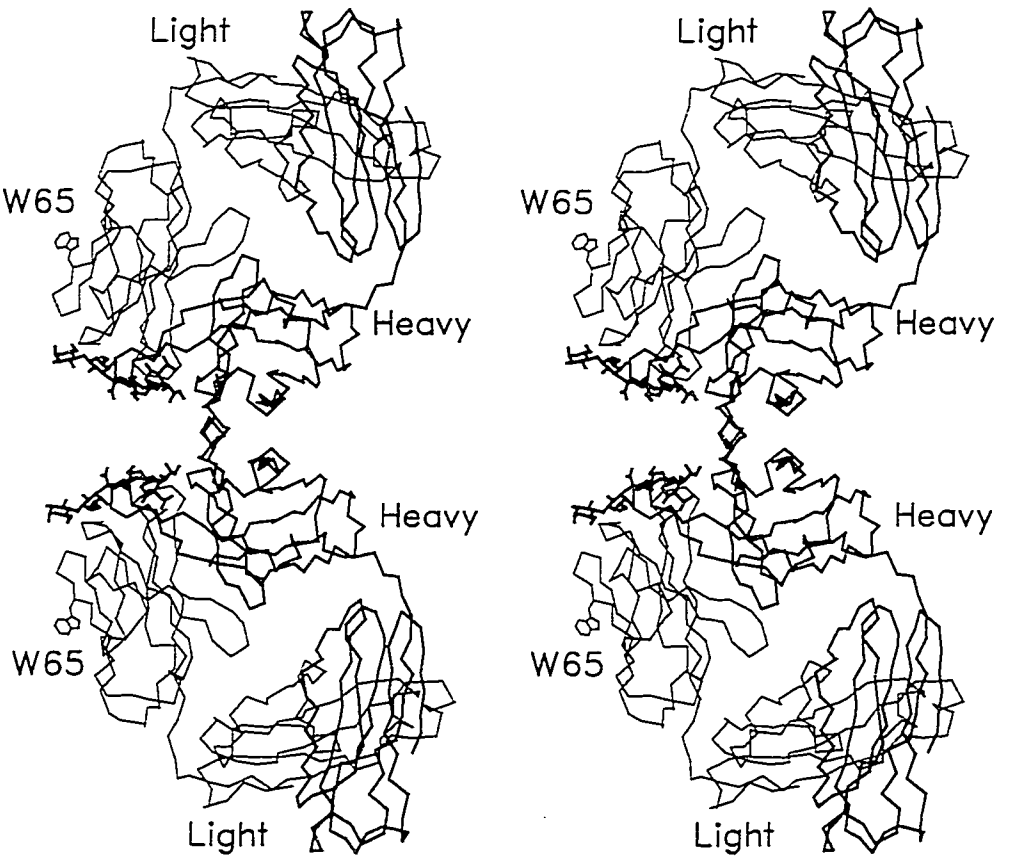

Figure 33: Light chain residue 65 position in the chR24 dimer. SETOR stereo representation of the chR24 dimer (heavy chains in black, light chains in gray), showing the GD3 model (red), and the position of the tryptophan residue at position 65 in the light chain. This tryptophan may aid in the stabilization of the light chain against the cell membrane.

Fabs stem from differences between their constant regions. The strong binding of murine R24 to GD3-liposomes can be attributed to homophilic binding between molecules of R24 and the formation of a multivalent antibody lattice. The reduced binding levels displayed by chR24 IgG reveals the strong participation of the constant regions of murine R24 in homophilic binding. Since the structures of the Fvs of R24 and chR24 have been shown in this study not to be significantly different, the differences in activity must be due to the change in constant regions from murine IgG3(κ) to human IgG1(κ). Similar differences in antibody affinities which accompany changes in constant region subclasses have been reported (Cooper *et al.*, 1994), and are attributed largely to the ability of murine IgG3 antibodies to form multivalent lattices. However the chimeric IgG still displays some homophilic binding, despite the human IgG1 heavy chain. The loss of homophilic binding in chR24 has been previously shown to occur in various V_H mutants, leading to the definition of ID_{HOM} (see 4.2.7, above), with the levels of homophilic binding displayed by the chR24 IgG to be directly attributable to interactions through the ID_{HOM}.

The difference in binding carries on to the Fab molecules of the murine and chimeric R24 IgG, with the murine Fab showing superior homophilic binding ability. Like their parent molecule, the Fabs of murine IgG3 antibodies display the ability to form divalent species through the constant domains.. This murine Fab behaviour was seen in the crystallization trials where the protein was found to be less soluble than the Fab from chR24 (6 vs 15 mg/mL)

4.3.3 Antigen-antibody matrix

Given that each mAb is bivalent both in antigen and homophilic binding, it is clear that binding of R24 to GD3-bearing surfaces would lead to the formation of antibody networks, which effectively increases the valency of the R24 antibody. The concentration of antibodies over a specific surface area would have the potential to increase immune response. Such networks could form only in the presence of significant amounts of membrane-bound GD3, and would explain why R24 targets transformed cells, while passing over cells displaying normal levels of GD3. The apparent flexibility of the β-sheet interaction (approximately 20° of freedom about the long axis of the interface), combined with the known flexibility of IgG molecules generally, would allow for the contours of cell membranes, and minimize stress on the antigen-antibody and homophilic interactions. A schematic of the cross-linked antibody-antigen network model is shown in Figure 34.

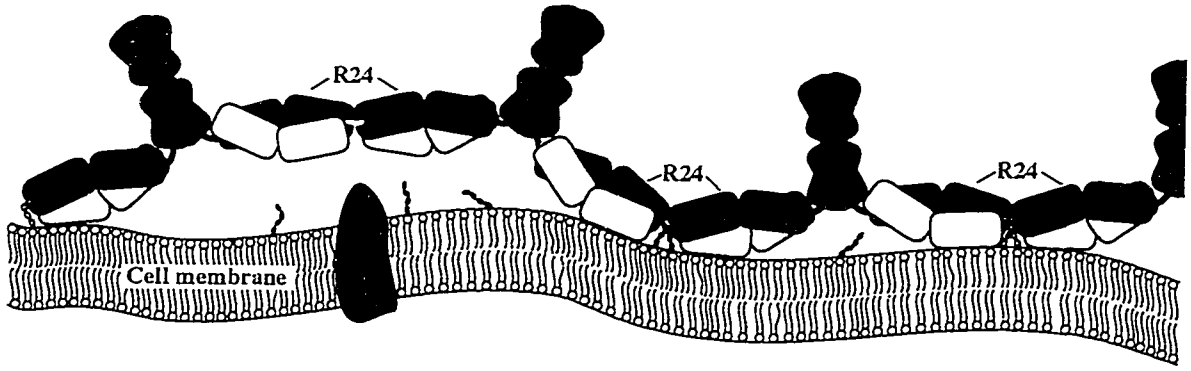

LATTICE MODEL

Figure 34: Antibody-Antigen network model. Model of the formation of an chR24 mAb lattice on the membrane of transformed cells expressing large amounts of ganglioside GD3. Molecules of R24 or chR24 (white and blue) are able to simultaneously bind GD3 antigen (red), other molecules of R24, and interact with the membrane surface (black) through the variable domain of the light chain. The large number of cooperative interactions stabilize the formation of an R24 lattice on the cell surface, which increases the effective valency of the antibody.

5 CONCLUSIONS:

R24 and chR24 specificity domains have nearly identical structures, including the location, size and shape of the antigen binding pocket. Most differences in the two structures can be accounted for by coordinate-errors from the lower resolution of the R24 structure. The antigen binding region is defined mostly by the three heavy chain CDRs, and has a defined structure with a deep pocket surrounded by a pronounced mouth.

The GD3 antigen model terminal sialic acid residue can penetrate to the bottom of the GD3-specificity pocket;; and the antigen model forms a number of hydrogen bonds, and shows a good surface interaction complementarity. The putative BEC2 antigenic determinant, found on the extended loop conformation of CDR L1, contains a LDSDG sequence which can be modelled into the binding pocket. The peptide model can form hydrogen bonds with the R24 pocket, and shows a similar surface complementarity as the GD3. The basis of mimicry between the BEC2 and GD3 antigen models is based on size and shape similarities, van der Waals and hydrogen bonding interactions, however no model of complementary charge dispersion was found. The loss of ID_{GD3} in all but one S53 mutant has been modelled to be caused by occlusion of the pocket by the mutant residue side chains. S53T mutation modifies the surface of the pocket but does not occlude the mouth enough to prevent GD3 specificity.

The structural basis for the homophilic binding is an uncommon head to head interaction forming an antiparallel β-sheet two R24 molecules. This interaction extends the antiparallel β-sheet of each of the V_H domains of the two antibodies involved. The region which expresses this homophilic binding epitope is found on the H2 framework

region proximal to the GD3 binding domain. This ID_{HOM} consists of residues 56-60, which form 4 hydrogen bonds between molecules, involving residues S56, I58 and Y60, and several side chain interactions. The proximity of the homophilic binding site to the GD3 binding pocket is critical due to the loss of homophilic binding through mutations at residue S53. The strucutral basis for the loss of ID_{HOM} is less clear than that of ID_{GD3} however mutations at S53 may disrupt homophilic binding by altering the H2 β-framework structure from canonical type 3 to type 2, or by the modification in the overall antibody-antigen interaction in such a way as to preclude the antibodies from coming into orientation required for ID_{HOM} contact. Modification of residue 61 has little effect on homophilic binding since this residue is outside of the β-sheet forming region. Thus main chain, side chain interactions and Canonical type 2 structure of H2 are required for homophilic binding. Only one other Fab structure shows the H2 β-sheet homophilic interaction, that of antibody HIL raised against an unspecified melanoma antigen.

The homophilic binding is quite labile and does not form extended interactions in solution. The dimer crystal structure however has led to a model of extended cross-linked matrix of R24 and chR24 on the surface of GD3 expressing cells. This matrix consists of R24 or chR24 bound to GD3 and bound to each other, and is responsible for the therapeutic effectiveness of R24. The stabilization of the R24-GD3 binding at the cellular membrane may be aided by the presence of W65 on the light chain which could intercalate into the lipid bilayer. The differences in the binding properties of murine R24 and chR24 and their respective Fabs are due to the changes in the constant domains in the chimeric antibody. Thus strong stable binding of GD3 by R24 is a cooperative process

requiring both V_H-V_H interactions and Fc-Fc interactions, with the antigen presented immobilized and in significant concentration on a membrane.

REFERENCES

Albino, A.P., A.N. Houghton, M. Eisinger, J.S. Lee, R.R.S Kantor, A.I. Oliff, and L.J. Old. 1986. Class II histocompatibility antigen expression in human melanocytes transformed by Harvey murine sarcoma virus (Ha-MSV) and Kirsten MSV retroviruses. *J. Exp. Med.* **164**:17-1722.

Bernstein, F.C., T.F. Koetzle, G.J.B. Williams, E.F. Meyer Jr., M.D. Brice, J.R. Rodgers, O. Kennard, T. Shimanouchi, and M. Tasumi. 1977. The Protein Data Bank: a computer-based archival file for macromolecular structures. *J. Mol. Biol.* **112**: 535-542.

Blundell, T.L. and L.N. Johnson. 1976. Protein Crystallography. Academic Press, New York. 90-97.

Boon, T. 1993. Tumor antigens recognized by cytolytic T lymphocytes: present perspectives for specific immunotherapy. *Int. J. Cancer* 54:177-180.

Brünger, A.T. 1992. "X-PLOR Manual, Version 3.0." Yale University Press, New Haven, Connecticut.

Carter, Jr. C.W. and C. W. Carter. 1979. Protein crystallization using incomplete factorial experiments. *J. Biol. Chem.* **254**: 12219-12223.

Carubia, J. M., R.K. Yu, L. J. Macala, J.M. Kirkwood, and J.M. Varga. 1984. Gangliosides of normal and neoplastic human melanocytes. Biochem. *Biophys. Res. Comm.* **120**: 500-504.

Caulfield, J., B. Barna, S. Murthy, R. Tubbs, J. Sergi, S. Mendendorp, and R.M. Burkowski. 1990. Phase Ia-Ib of an anti-GD3 monoclonal antibody in combination with interferon-a in patients with malignant melanoma. *J. Bio. Response Mod.* **9**: 319-328.

Chapman, P.B., M. Longberg and A.N. Houghton. 1990a. Light chain variance of an IgG3 anti-GD3 monoclonal antibody and the relationship between avidity, effector functions, tumor targeting, and antitumour activity. *Cancer Res.* **50**: 1503-1509.

Chapman, P.B., H. Yuasa, and A.N. Houghton. 1990b. Homophilic Binding of Mouse Monoclonal Antibodies Against GD3 Ganglioside. *J. Immun.* **145**: 891-898.

Chothia, C., and A.M. Lesk. 1987. Canonical Structures for the Hypervariable Regions of Immunoglobulins. *J. Mol. Biol.* **196**: 901-917

Chothia C., A.M. Lesk, A. Tramontano, M. Levitt, S.J. Smith-Gill, G. Air, S. Sheriff, E.A. Padlan, D. Davies, W.R. Tulip, P.M. Colman, S. Spinelli, P.M. Alzari, and R.J. Poljak. 1989. Conformations of immunoglobulin hypervariable regions. *Nature* **342**: 877-883.

Cole, D.J., D.P. Weil, J. Shilyansky, M. Custer, Y. Kawakami, S.A. Rosenberg and M.I. Nishimura. 1995. Characterization of the functional specificity of a cloned T-cell receptor heterodimer recognizing the MART-1 melanoma. *Cancer Research* **55**:748-752

Connolly, M.L. 1983. Analytical Molecular Surface Calculation. *J. Appl. Cryst.* **16**: 548-558.

Cooper, L.J.N., D. Robertson, R. Graznow, and N.S. Greenspan. 1994. Variable domain-identical antibodies exhibit IgG subclass-related differences in affinity and kinetic constants as determined by surface plasmon resonance. *Mol. Immunol.* **31**: 577-584.

Dippold, W.G., K.O. Lloyd, L.T.C. Li, H. Ikeda, H.F. Oettgen and L.J. Old. 1980. Cell surface antigens of human malignant melanoma: Definition of six antigenic systems with mouse monoclonal antibodies. *Proc. Natl. Acad. Sci.* 77(10): 6114-6118.

Evans, S.V. 1993. SETOR: Hardware lighted three-dimensional representations of macromolecules. *J. Mol. Graphics* **11**: 134-138.

Goding, J.W. 1983. Monoclonal Antibodies: Principles and Practice.

Guddat, L.W., L. Shan, J.M. Anchin, D.S. Linthicum and A.B. Edmundson. 1994 Local and transmitted conformational changes of an anti-sweetener Fab. *J. Mol. Biol.* **236**:247-274.

Hahn, G.S. 1986. Immunoglobulin-derived drugs. *Nature.* **324**: 283-284.

Hahn, T. (Ed.). 1989. International Tables for Crystallography. Volume A: Space-group Symmetry. D. Reidel Publishing Company, Boston.

Hakomori, S. 1981. Glycosphingolipids in cellular interaction, differentiation, and oncogenesis. *Ann. Rev. Biochem.* **50**: 733-64.

Hamburger, R.N. 1975 Peptide inhibition of the Prausnitz-Kustner reaction. *Science.* **189**: 3889.

Hamilton, W.B., F. Helling, K.O. Lloyd, and P.O. Livingston. 1993. Ganglioside expression on human malignant melanoma assessed by quantitative immune thin-layer chromatography. *Int. J. Cancer* **53**: 566-573.

Hirabayashi, Y., H. Higashi, S. Kato, M. Taniguchi and M. Matsumoto. 1987. Occurrence of tumour associated ganglioside antigens with Hanganutziu-Deicher antigenic activity on human melanomas. *Japan. J. Cancer Res.* **78**: 614-620.

Irie, R.F., and M.H. Ravindranath. 1990. Gangliosides as targets for monoclonal antibody therapy of cancer. In Therapeutic Monoclonal Antibodies. C.A.K Borreback and J.W. Larric, editors. Stockton Press, New York. 75-85.

Jancarik, J. and Kim, S.H. 1991.Sparse matrix sampling: a screening method for crystallization of proteins. *J. Appl. Cryst.* **24**: 409-411.

Jerne, N.K. 1974. Towards a network theory of the immune response. *Ann. Immunol. (Paris)* **125C**: 373-389

Jones, T.A. 1978. A Graphics Model Building and Refinement System for Macromolecules. *J. Appl. Cryst.* **11**: 268-272.

Karlsson, R., A. Michaelsson, and L. Mattsson. 1991. Kinetic analysis of monoclonal antibody-antigen interactions with a new biosensor based analytical system. *J. Immunol. Methods.* **145**: 229-240

Lescar, J., M. Pellegrini, H. Souchon, D. Tello, R.J. Poljak, N. Peterson, M. Greene, and P.M. Alzari. 1995. Crystal structure of a cross-reactive complex between Fab F9.13.7 and Guinea Fowl Lysozyme. *J. Biol. Chem.* **270**(30): 18067-18076.

Lenert, P., D. Kroon, H. Spiegelberg, E.S. Golub, and M. Zanetti. 1990. Human CD4 binds immunoglobulins. *Science* 248: 1639-1643.

Lloyd, K.O. 1993. Tumour antigens known to be immunogenic in man. In Specific Immunotherapy of Cancer with Vaccines. J-C. Bystryn, S. Ferrone, and P. Livingston, editors. The New York Academy of Sciences, New York. 50-58.

LoBuglio, A.F., R.H. Wheeler, J. Trang, A. Hanes, K. Rogers, E.B. Harvey, L. Sun, J. Ghrayeb, and M.B. Khazaeli. 1989. Mouse/human chimeric monoclonal antibody in man: Kinetics and immune response. *Proc. Natl. Acad. Sci. USA.* 86: 4220-4224.

MacCallum, R.M., A.C. Martin, J.M. Thornton. 1996. Antibody-Antigen interactions: contact analysis and binding. *J. Mol. Biol.* **262**(5): 732-45.

McPherson, A. 1985. Crystallization of macromolecules: general principles. *Methods in Enzymology.* **114**: 112-120.

McRee, D.E. 1993. Practical Protein Crystallography. Academic Press, Inc, Toronto.

33-37, 51-55.

Nicholls, A. K.A. Sharp, and B. Honig. 1991 Protein folding and association: insights from the interfacial and thermodynamic properties of hydrocarbons. *Proteins: Structure, Function and Genetics.* **11**(4): 281-296.

Ortaldo, J.R., A.T. Mason, D.L. Longon, M. Beckwith, S.P. Creekmore, and D.W. McVicar. 1996. T cell activation via the disialoganglioside GD3: analysis of signal transduction. *J. Leuk. Bio.* **60**(4):533-539.

Otwinowski, Z and Minor, W. 1996. Processing of X-ray diffraction data collected in oscillation mode, in Methods in Enzymology 276, C.W. Carter, Jr. and R.M. Sweet, Eds., Academic Press.

Padlan, E.A. 1994. Anatomy of the antibody molecule. *Molecular Immunology* **31**(3): 169-217.

Prenner, B.M. 1987. Double-blind placebo-controlled trial of intranasal IgE pentapeptide. *Ann. All. Res.* **58**: 332-335

Poljak, R.J. 1973. X-Ray Crystallographic Studies of Immunoglobulins. *Contemporary Topis. in Molecular Immunology* **2**: 1-26.

Pukel, C., K.O. Lloyd, L.R. Travassos, W.G. Dippold, H.F. Oettegen, and L.J. Old. 1982. GD3, a prominent ganglioside of human melanoma. Detection and characterization by mouse monoclonal antibody. *J. Exp. Med.* **155**: 1133-1147.

Raymond, J., J. Kirkwood, D. Vlock, M. Rabkin, R. Day, T. Whiteside, R. Herberman, R. Mascari, and B. Simon. 1991. A phase Ib trial of murine monoclonal antibody R24 (anti-GD3) in metastatic melanoma. *Proc. Am. Soc. Clin. Oncol.* **10**: 298.(Abstr.)

Saul, F., and R.J. Poljak. 1992. Crystal Structure of the Fab fragment from the human myeloma immunoglobulin IgG HIL at 1.8 angstroms resolution. Structure deposited in Protein Data Bank, Chemistry Department, Brookhaven National Laboratory, Upton, NY 11973. Assession number: 8FAB.

Seymour, G.J., N.W. Savage, and L.J. Walsh. 1995. Immunology: An Introduction for the Health Sciences. McGraw-Hill Book Company Australia Pty Limited. 11-41

Sheriff, S., C.Y. Chang, P.D. Jeffrey, and J. Bajorath. 1996. X-ray structure of the complexed anti-tumour antibody BR96 and comparison with its antigen-bound form. *J. Mol. Biol.* **295**: 938-946

Stout, G.H. and L.H. Jensen. 1989. X-Ray Structure Determination: A Practical Guide. John Wiley and Sons, Toronto. 20-51

Thurin, J., M. Herlyn, O. Hindsgaul, N. Stromber, K.A. Karlsson, D. Elder, Z. Stepleski, and H. Koprowski. 1985. Proton NMR and fast-atom bombardment mass spectrometry analysis of the melanoma associated ganglioside 9-O-acetyl-GD3. *J. Biol. Chem.* **620**: 14556-14563.

Tizard, I.R. 1984. Immunology, an introduction. Saunders College Publishing, Philadelphia.

Vadhan-Raj, S., C. Cordon-Cardo, E.A. Carswell, D. Mintzer, L. Dantis, C. Duteau, M.A. Templeton, H.F. Oettgen, L.J. Old, and A.N. Houghton. 1988. Phase I trial of a mouse monoclonal antibody against GD3 ganglioside in patients with melanoma: Induction of inflammatory response at tumour sites. *J. Clin. Oncol.* **6**:1636-1648.

Yamaguchi, Y., H. Kim, K. Kato, K. Masuda, I. Shimada, Y. Arata. 1994. Proteolytic fragmentation with high specificity of mouse immunoglobulin G. Mapping of proteolytic cleavage sites in the hinge region. *J. Imm. Meth.* **181**: 259-267.

Yan, X., S.V. Evans, M.J. Kaminski, S.D. Gillies, R.A. Reisfeld, A.N. Houghton, and P.B. Chapman. 1996. Characterization of an Ig V_H Idiotope that results in specific homophilic binding and increased avidity for antigen. *J. Imm.* **157**:1582-1588.

Woolfson, M.M. 1970. An Introduction to X-Ray Crystallography. Cambridge University Press, New York.

Wu, T.T. and E.A. Kabat. 1970. An analysis of the sequences of the variable regions of Bence Jones proteins and myeloma light chains, and their implications for antibody complementarity. *Ann. N.Y. Acad. Sci.* 190:371-381

IMAGE EVALUATION TEST TARGET (QA-3)

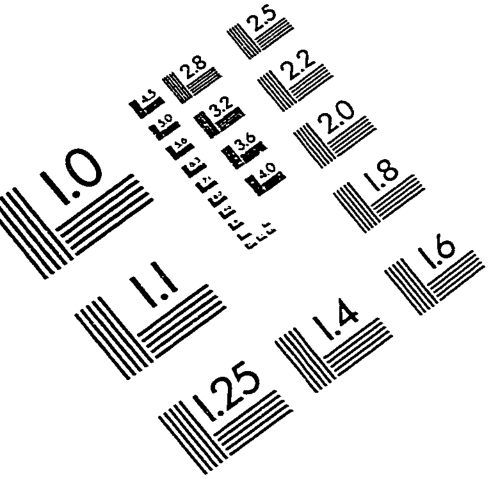

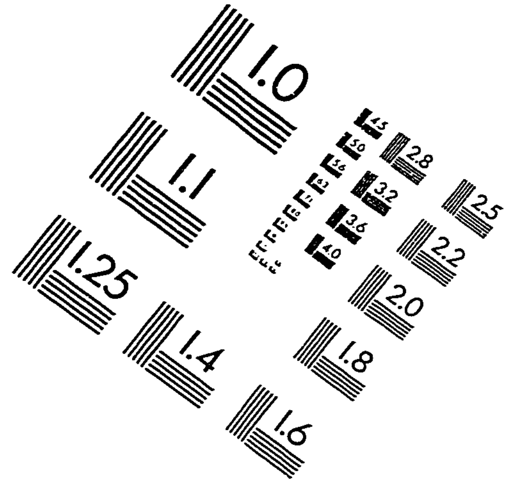

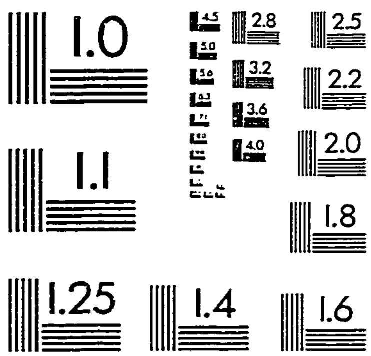

150mm

6″

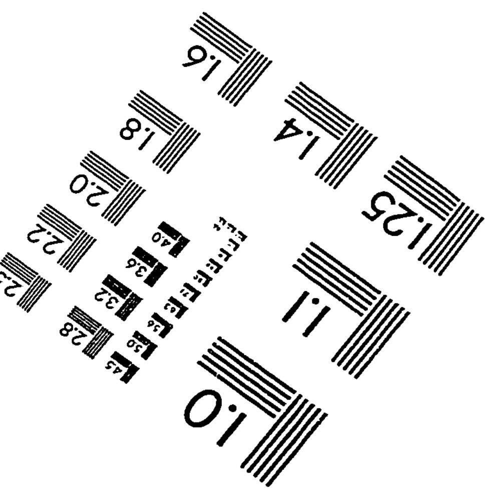

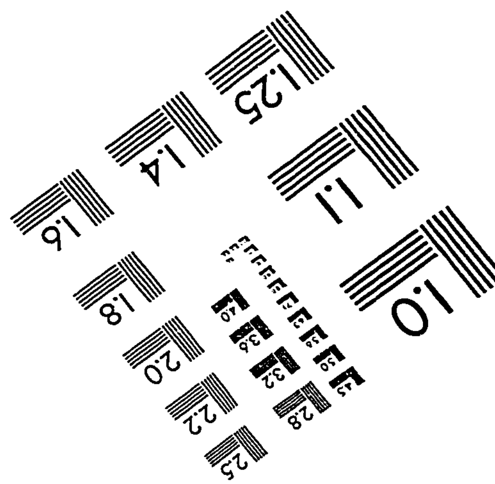

APPLIED IMAGE, Inc
1653 East Main Street
Rochester, NY 14609 USA
Phone: 716/482-0300
Fax: 716/288-5989